UNIVERSITÀ DEGLI STUDI DI PADOVA

DIPARTIMENTO DI TECNICA E GESTIONE DEI SISTEMI INDUSTRIALI

CORSO DI LAUREA MAGISTRALE IN INGEGNERIA DELL'INNOVAZIONE DEL PRODOTTO

TESI DI LAUREA

Mechanical characterization of a ballistic steel in the presence of a notch

Relatore: Prof. Filippo Berto

Correlatore: Prof. David Ángel Cendón Franco

Laureando: Filippo Faccio

Anno Accademico 2014-2015

Introduction

Little excursus about material under stress

It is assumed that the reader is familiar with some basic theory regarding the mechanical properties of materials, as can be found in textbooks such as Ashby and Jones' *Engineering Materials* (2005) or Hertzberg's *Deformation and Fracture Mechanics of Engineering Materials* (1995), and also with the fundamentals of solid mechanics and fracture mechanics, for which many useful textbooks also exist (Broberg, 1999; Janssen et al., 2002; Knott, 1973). It concerns, in general, the deformation and failure of materials under stress, but emphasis will be placed on those types of failure which will be the main subjects of brittle fracture. Of special interest from a mechanics point of view will be the U-notches geometry under mode I and mixed mode, which give rise to stress concentrations and stress gradients. In this respect, the use of computer-based methods such as finite element analysis (FEA) will also be discussed.

Failure at the atomic level

The study of failure mechanisms in materials has a tendency to get complicated, so it is worth remembering that, at the smallest scale, there are only two mechanisms by which materials can break, which I will call *cleavage* and *tearing*. Cleavage involves the fracture of atomic bonds; a crack can form by breaking the bonds linking two parallel planes of atoms, and this crack can then grow by the fracture of successive bonds new the crack tip, essentially unzipping the material in directions corresponding to atomic lattice planes. The fracture surface consists of a series of flat facets corresponding to the grains of the material. Tearing, on the other

hand, occurs when material separates due to plastic deformation: atoms move around to create high levels of strain so that the material literally tears itself apart. This can manifest itself in various different ways, from macroscopic thinning (necking) or sliding (shearing) of material to microscopic void formation and growth. These two atomic failure mechanisms are often referred to as 'brittle' and `ductile'; however, we have avoided using these terms because they are also used with different meanings to describe failure modes at the macroscopic scale as discussed below.

Failure modes in engineering components

The failures of engineering components and structures are caused by one of seven different modes: elastic, ductile, brittle, fatigue, stress-corrosion, creep, and wear.

Elastic failures are those failures which occur as a result of a low value of Young's modulus, *E.* Two types of elastic failure can be mentioned. The first is excessive deflection, which may prevent the correct functioning of a structure examples include bridges and vehicle suspensions. The second is buckling, by which, at a certain critical combination of load and elastic modulus, the deflections of a structure become unstable so that small deviations become magnified. A classic example is the collapse of a thin column loaded in compression.

Ductile fracture is the term used to describe failure occurring due to macroscopic plastic deformation; the material's yield strength is exceeded over a large region so that plastic strain can occur throughout the load-hearing section, causing either fracture or a major change in shape so that the component can no longer function. In principle the prediction of this type of failure is simple; since the only consideration is that the stress in the part should exceed the yield strength. In practice, however, the spread of plasticity and the resulting redistribution of stresses and strains make

the prediction of plastic collapse loads a difficult analytical problem. For complex engineering structures, solutions are usually obtained using FEA and other computer simulations.

Brittle fracture refers to failures which occur as a result of rapid crack propagation. The crack in question may already exist. For example in the form of a manufacturing defect or slowly growing fatigue crack, or it may form as a result of local high stresses, for example near a notch. Once formed, the crack is able to grow, if the applied loads are high enough, by fracture of material near its tip. This material may fail by either cleavage or tearing. In classic brittle fracture, the process of crack growth is unstable, leading to almost instantaneous failure of the component. In such situations any plastic deformation is confined to the immediate vicinity of the crack, so there may be little sign of macroscopic plasticity. This simple distinction between ductile fractures is complicated by the fact that intermediate situations can often arise: crack growth can occur more slowly and gradually, requiring a monotonically increasing load, if there is a significant amount of plasticity or damage near the crack tip. The study of crack propagation has created the science of Fracture Mechanics, which will be discussed in more detail below.

Fatigue is a process of crack initiation and growth, which occurs as a result of cyclic loading. A regular cycle of stress, such as a sine wave, can be described using two parameters: the stress range $\Delta\sigma$ and the mean stress σ_{mean}. Another common descriptor is the load ratio *R*, defined as the ratio of the minimum and maximum stresses in the cycle:

$$R = \sigma_{min}/\sigma_{max}$$

The most common type of fatigue test involves applying a cyclic stress to a test specimen and counting the number of cycles to failure N_f . Separation will occur when a crack has grown to such a sufficient length that it causes a ductile or brittle fracture of the remaining cross section: some workers prefer to define failure as the creation of a crack of a specified size, usually a few millimeters. The typical stress-life curves, describing the dependence of N_f on $\Delta\sigma$ and σ_{mean} like a descending curve. In some materials the curve becomes effectively horizontal for N_f values in the range 10^6-10^7 cycles, allowing one to define a *fatigue limit,* $\Delta\sigma_{o.}$ Often, however, there is no clear asymptote in which case the fatigue limit is defined at a specified number of cycles, which is often called the *fatigue strength.*

Stress-corrosion cracking (SCC) is a form of gradual failure which is rather like fatigue in that it precedes by crack initiation and gradual propagation. However, in this ease the crucial factor is not a cyclic stress but the existence of a corrosive chemical environment. The mechanisms of SCC are many and varied but usually involve some kind of synergistic action between the chemical process and the applied stress.

Creep is a process of plastic deformation that occurs gradually. In fact all plastic deformation processes are thermally activated, proceeding more easily as the temperature is increased towards the material's melting point. Creep failures can also involve the creation and growth of crack-like damage.

Wear is the general name given to tribological failures, failures which occur due to the rubbing action between two surfaces. If compressive stress and a sliding (shear motion) occur across a material interface, very high local stresses will arise due to small surface irregularities, creating conditions in which material can be removed from one or both surfaces. There are various mechanisms of wear. The one that will

be of most interest to us is known as *contact fatigue* and involves the creation of cracks at or near the point of contact. These cracks can grow to cause removal of surface material by spalling, for example in gear teeth. If there are also cyclic body forces in the component, then cracks which are initiated by contact fatigue can subsequently grow into the component by conventional fatigue processes. This type of failure is known as *fretting fatigue.* The prediction of tribologically induced failures such as these is difficult because of the problems involved in estimating local stresses, which are affected by surface roughness, surface deformation and lubrication.

Stress Concentrations

It is almost inevitable that, in any engineering component, stresses will vary from place to place, and that failure will occur in locations where stresses are relatively high. One can think of a few exceptions to this rule (wires and tie-bars under pure tensile loading, for example) but apart from these we can say that the phenomenon of stress concentration is responsible for all mechanical failures in practice. Stress concentration has two causes: loading and geometry. Loading modes which cause stress gradients include bending and torsion, both of which tend to concentrate stresses at the surface. However, this type of stress concentration is generally very mild in comparison to the effect of geometric features such as holes, corners, bends and grooves.

It is important to remember another assumption analysis, which is that the material behaves as a homogeneous continuum. In practice, of course, materials are not continuous, a fact which had been suspected since the time of the Greek philosopher Leucippus (fifth century 13 BC), who first proposed that material is made up of atoms. Atomic structure is of course important, but for most

materials, properties such as strength and toughness are strongly affected by behavior at the microstructural level, where features such as grains, precipitates and inclusions exert both positive and negative effects. A fact which is often overlooked is that if we examine stress and strain fields at this small scale, we find that they are strongly inhomogeneous, affected by microstructural parameters such as local grain orientation, disparities in the elastic stiffness of different phases, and the properties of grain boundaries and other interfaces. Experimental measurements (Delaire et al., 2000) and computer models (Bruckner-Foil et al., 2004) have revealed the large extent of these local variations in stress and strain, which can be as high as a factor of 10. These effects may be of relatively little importance if the scale of the fracture process is much larger than any microstructural feature, in which case it may be satisfactory to think of the stresses calculated by continuum analysis as average quantities, ignoring their local variations.

Elastic Stress Fields for Notches and Cracks

The study of stress concentration effects is mostly carried out using notches. As the following figure shows, a notch can be defined by three parameters: its depth *D,* root radius *p* and opening angle 2α. To be precise one should add a fourth feature, the notch shape, to include the fact that the sides of the notch can have different amounts of curvature.

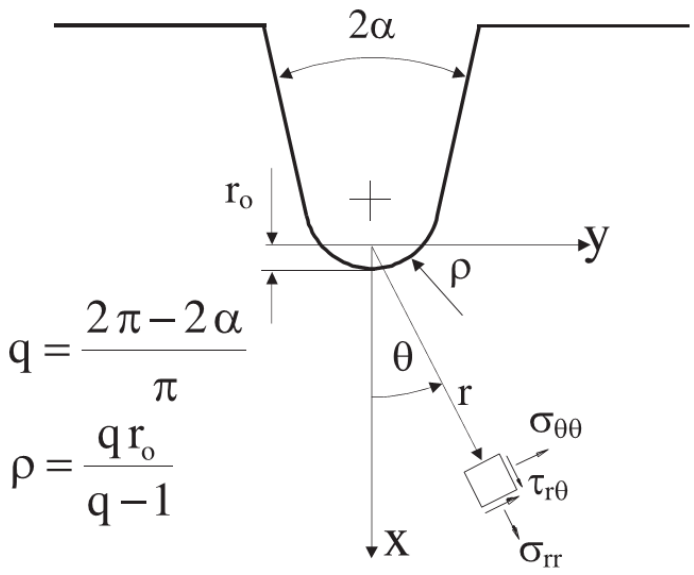

Figura 1

However, in practice the two features which mostly control stress concentration are *D* and *ρ,* with notch angle having a secondary effect which becomes significant at large values ($2\alpha > 90°$). Coordinates centered on the point of maximum stress, at the notch root are normally used in notch stress fields, Figure 1 shows a polar coordinate system *(r, θ)*.

The reason that researchers use notches to study stress concentration effects is because they are relatively simple to make, simple to test experimentally and to analyses theoretically. However, it should not be forgotten that the real purpose in doing all this is to predict the behavior of stress concentration features in engineering structures and components, which can be geometrically much more complex.

To return to notches, some simple analytical solutions exist in certain cases. For example, the stress field created by a circular hole in a body of infinite size can be described as a function of applied nominal stress σ and hole radius a_h. For the case of $\theta = 0$ the result is:

$$\sigma_{\theta\theta} = \sigma\left(1 + \frac{1}{2}\left(\frac{a_h}{r + a_h}\right)^2 + \frac{3}{2}\left(\frac{a_h}{r + a_h}\right)^4\right)$$

$$\sigma_{rr} = \frac{3\sigma}{2}\left(\left(\frac{a_h}{r + a_h}\right)^2 + \left(\frac{a_h}{r + a_h}\right)^4\right)$$

In this case $\sigma_{\theta\theta}$ is the tensile stress in the circumferential direction and σ_{rr} the tensile stress in the radial direction. This is a two-dimensional (2D) analysis; stresses can also arise in the thickness (z) direction, depending on the degree of constraint: this will be considered below in the section on Fracture Mechanics. Note that for this hole, as for any notch; stresses arise not only in the direction of the applied tension, but also in other directions, creating in general a complex three-dimensional (3D) stress field. The effects of these other stresses can be important on multiaxial loading.

The maximum value of $\sigma_{\theta\theta}$ (occurring at $r = 0$) is 3σ, giving a stress concentration factor of $K_t = 3$, for a circular hole. Stress concentration factors, determined by an analytical solution, a computer simulation or an experimental stress analysis, have been recorded for many different types of notches and other features (see, for example, Peterson, 1974). One useful result, strictly only valid for elliptical holes but reasonably accurate for most notches, gives K_t as a function of notch depth D (equal to the length of the semi-major axis of the ellipse) and root radius ρ (defined at the point of minimum radius) as:

$$K_t = 1 + 2\sqrt{\frac{D}{\rho}}$$

Creager and Paris developed a simple equation to describe the stress-distance curve, ahead of a narrow slot that is a notch in which ρ«D (Creager and Paris, 1967),

which we will make considerable use of in later chapters. In the limit where $\rho = 0$ we have a crack, and in this case, the stress field can also be predicted analytically. The K_t factor becomes infinite; the result for stress $\sigma(r)$ as a function of distance r from the crack tip, for a through-thickness crack of half-length a in an infinite body subjected to tensile stress σ, is (Westergaard, 1939)

$$\sigma(r) = \frac{\sigma}{\left[1 - \left(\frac{a}{a+r}\right)^2\right]^{1/2}}$$

Here $\sigma(r)$ is the tensile stress in the same direction as the applied stress. This is also the perpendicular direction to the applied crack faces, so this stress is often referred to as the crack-opening stress, which is usually the most important stress controlling crack propagation. For points close to the crack tip (i.e. $r \ll a$):

$$\sigma(r) = \sigma\sqrt{\frac{a}{2r}}$$

Combining the stress and the crack length we can define the stress intensity K as:

$$K = \sigma\sqrt{\pi a}$$

The convenience of this definition, and the reason for the insertion of the constant π will be explained in the following section. Now the stress field depends only on K and

a: this result is only true for the particular geometry of an infinite body containing a straight, through-thickness crack. However, it turns out that, for many other eases, the previous statement retains its same general form with the inclusion of a constant *F:*

$$K = F\sigma\sqrt{\pi a}$$

In this equation, *F* is a function of various parameters including crack shape location and the type of loading. Values for *F* have been calibrated for many cases of interest (e.g. Murakami, 1987).

For notches in which $\rho = 0$ but $\theta > 0$ (sharp, V-shaped notches), it retains the same general form, but the dependence on *r* changes:

$$\sigma(r) = \Psi r^{-\lambda}$$

Here Ψ has the same meaning as *K* except that the square root is replaced by the exponent (-λ), whose value is a function of θ (Williams, 1952). As a general problem, the full analytical description of stress fields for notches, especially in bodies of finite width, presents significant challenges. However, useful solutions have been obtained for various cases (Atzori et al., 2001; Filippi and Lazzarin, 2004). In practice, closed-form solutions cannot be determined for most of the stress concentration features which exist in components, but fortunately this information can now be obtained using computer simulations such as FEA.

Fracture Mechanics

Fracture mechanics is the science which describes the behavior of bodies containing cracks. It is one of the most important developments in the entire field of mechanics. The great success of fracture mechanics has been to show that, under certain well-defined conditions, the propagation of the crack can be predicted using some very simple linear elastic analysis. When these conditions prevail, we enter the realm of Linear Elastic Fracture Mechanics (LEFM). I will first describe the basic theory of LEFM, leaving discussion of its limitations and assumptions for later. What follows is necessarily only a brief outline: for more detailed treatment I refer the reader to some of the excellent books which have been written on this subject (Broberg, 1999; Janssen et al., 2002; Knott, 1973).

We can predict the conditions which are necessary for brittle fracture, for slow crack growth by fatigue and for stress-corrosion cracking, assuming that a crack already exists. This is much simpler in the case of a crack than in the more general case of a notch. This is because all these fracture modes involve a cracking process; if a crack is not present then it will have to be created during the failure. On the other hand, if the crack is already there, we merely have to consider its propagation. Propagation can be defined as any increase in crack length, δa. If we consider the limit in which δa is vanishingly small, we can assume that there was no significant change in the stress conditions near the crack tip during propagation. We say that the crack extends under *steady state* conditions. A further simplifying assumption is that crack growth is under *local control*, by which we mean that the criteria for propagation can be entirely determined by stress conditions in the immediate vicinity of the crack tip. The opposite of local control is *global control*, which implies that other aspects, such as for example the type of remote loading being applied, influence crack behavior.

Within these limitations, the behavior of the crack can be described using the parameter *K*, the stress intensity, that it uniquely determines the magnitude of the stress field in the vicinity of a crack. The argument goes that two different cracks (e.g. cracks of different length and shape in different bodies) will have the same stress fields if *K* is the same for both; therefore if one crack can propagate, then so can the other. As pointed out in the previous section, this only applies to the stress fields close to the crack tip *(r «a;* hence the assumption of local control.

An alternative, and rather more persuasive, argument for the uniqueness of the *K* parameter is a thermodynamic one which was formulated by Griffith and further developed by Irwin (1964). This is a virtual work argument, in which we imagine a small amount of crack extension and compute the energy changes which occur. The problem can be simplified by assuming a so-called 'fixed grips' type of loading, in which the cracked specimen is held tightly between two loading grips which do not move during the experiment, so that there is no external work done on the specimen. Griffith proposed that the energy which is necessary for crack extension was equal to the energy needed to create the new surfaces, thus (for a through-thickness crack in a specimen of unit thickness) this is simply equal to $2\gamma(\delta a)$, where γ is the surface energy and the factor 2 arises because two surfaces are being created. In fact, even though this is an accurate estimate in the case of certain very brittle materials such as glass, crack propagation in most other materials requires more energy, due to various toughening mechanisms which operate in front of or behind the crack tip. We can lump these together to define a general crack-propagation term G_c, so that the energy for crack extension becomes $G_c(\delta a)$.

The energy which is available to drive crack propagation, in the absence of any external work, is the elastic energy released when the crack grows. This can be visualized as the energy released when atomic bonds near the crack tip are broken and, more importantly, when the strains in the surrounding atomic bonds are reduced. The

decrease in elastic energy, δW (per unit thickness), accompanying crack extension δa, can be shown as:

$$\delta W = \frac{\sigma^2}{E} \pi a \, \delta a$$

Equating this to $G_c(\delta a)$, we can find the stress needed for brittle fracture, that is the stress at which there will be just enough elastic energy stored in the body to drive crack propagation. This is the brittle fracture strength, σ_f; the result is

$$\sigma_f = \sqrt{\frac{G_c E}{\pi a}}$$

We note that fracture strength depends only on crack length and two material parameters, G_c and F; combining these we can rewrite the equation as:

$$\sigma_f = \frac{K_c}{\sqrt{\pi a}}$$

where K, is defined as:

$$K_c = \sqrt{G_c E}$$

We saw above that this parameter K can also be used to describe crack growth in fatigue. Here we use the range of stress intensity, ΔK, defined as:

$$\Delta K = F \Delta\sigma \sqrt{\pi a}$$

The crack growth rate (for a given R) is a function of ΔK and R. At values of K in the mid-range, the following equation (Paris, 1964) applies:

$$\frac{da}{dN} = A(\Delta K)^n$$

Here *A* and *n* are material constants for a given R. At low values, the line curves down to a threshold ΔK_{th} below which crack growth is negligible. Similar dependencies can also be defined for stress-corrosion cracking.

The above calculations all assumed that the crack was being loaded by a tensile stress applied perpendicular to its faces. This is certainly the most important case: compressive stresses, or tensile stresses applied in orthogonal directions (parallel to the crack faces or in the through-thickness direction) do not generally have any effect because they do not cause stress concentration; even though exceptions can occur in anisotropic materials.

However, local stress fields (and therefore, potentially, crack propagation) can occur due to shear loadings, applied parallel to the crack faces, in one of two orthogonal directions. Figure 2 illustrates the three important types of loading: simple tension (which is referred to as mode I), in-plane shear (mode II) and out-of-plane shear (mode III).

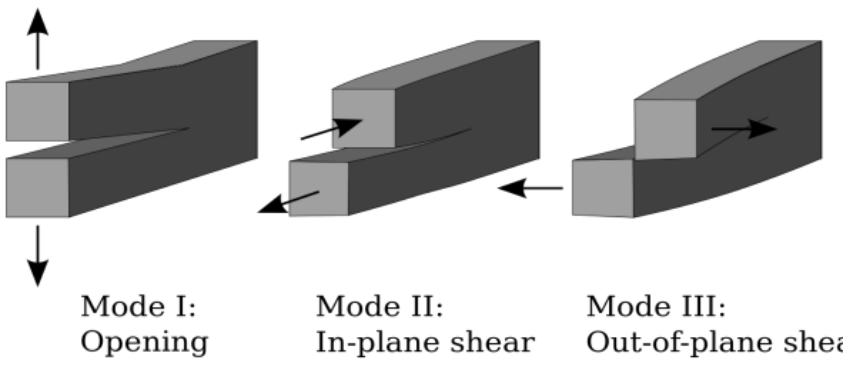

Figura 2 Different opening modes

The effect of constraint on fracture toughness

The above analysis assumed a body of constant thickness B but did not consider any particular values for that thickness. If B is small, plane stress conditions will occur, in which the through-thickness stress σ_z is zero. In thicker specimens, however, material near the crack tip in the center of the specimen will experience plane-strain conditions, in which σ_z is finite and varies with r. The net effect of this, especially for metals and other materials which develop plastic zones is that crack propagation is easier, and therefore K, is lower, when plane strain is present. Figure £ shows the typical variation of measured K_c with thickness:

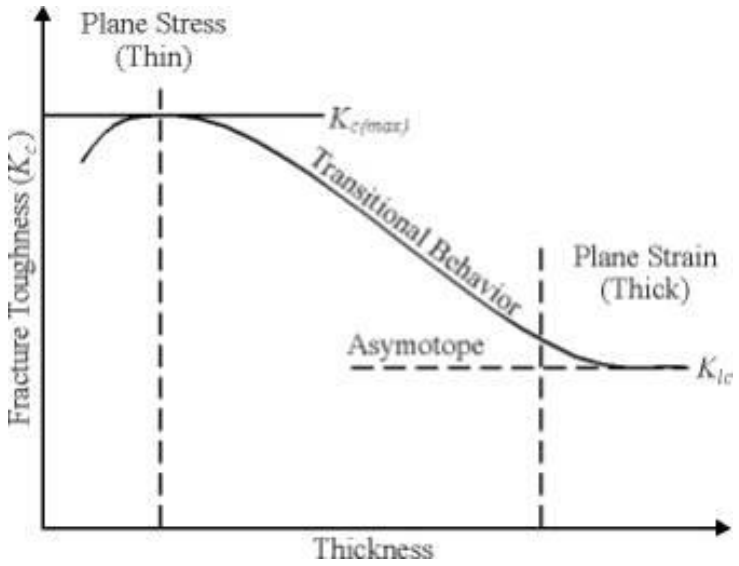

Figura 3 Fracture Toughness vs Thickness

The plane-strain toughness can be measured, provided B is sufficiently large. For thin specimens, the picture is more complicated. A reliable value of K_c is difficult to measure due to out-of-plane forces, and since it is certainly larger, one is more likely to encounter other limitations arising from the size of the plastic zone. For these reasons the plane-strain fracture toughness is the value which is generally measured and quoted. There is a convention by which this is distinguished using the symbol

K_{1c}, however this convention will not be used in this work; because; I will refer to the fracture toughness, however measured, as K_c.

However, the problem just described is actually only one, relatively simple, case of the more general problem of constraint. The change in stress pattern in thick specimens due to finite values of σ_z, is known as 'out-of-plane constraint'; in fact, stresses can also arise in the in-plane directions, which we can refer to as σ_{xx} and σ_y, these being directions parallel and perpendicular to the crack direction, respectively. We noted above that the stress field is a simplification of the true, 3D stress field. It turns out to be sufficiently accurate, provided failure occurs at relatively low applied stresses, but otherwise it ignores stress terms which become significant and which like σ_z, have real effects on the strength of the material.

Non-linear behavior: Plasticity and damage zones

The predicted stress fields often do not occur in practice because when stresses become very high locally, a number of other factors come into play. There are essentially three mechanisms, which modify stresses near the tip of a crack or notch. Firstly, elastic behavior may become non-linear: this is generally not taken into account, though it may have significant modifying effects, especially in certain polymers and ceramics. Secondly, yielding may occur, creating a plastic zone. Thirdly, the high stresses may cause damage, for example in the form of microscopic cracks or delamination, creating a damage zone. The term 'process zone' is sometimes used as a describe the region near the stress concentration feature in which any of these term to describe the region near the stress concentration feature in which any of these non-linear processes are occurring (though some workers use this term to mean only the zone in which fracture is occurring).

The effect of these non-linear processes is to reduce peak stress in any situation where there is a stress gradient, including plain beams in bending or torsion as well as stress concentration features. The details of the stress field inside the plastic zone or damage zone are difficult to estimate, since they depend on the precise mechanisms which are operating and how these mechanisms are affected by the 3D stress field. For example, stresses rise considerably higher in a plastic zone which is subjected to high constraint, due to suppression of yielding, because yielding is controlled by shear stress and thus by differences between the three principal stresses.

Failure, when it occurs, is invariably initiated within the zone of plasticity or damage. An existing crack may extend, a crack may form at the root of an existing notch, alternatively cracks may form elsewhere in the process zone and link hack to the main crack or notch. In many cases the detailed processes of failure at the microscopic level are still poorly understood. What is clear, however, is that materials which have high toughness invariably form large zones of plasticity or damage before failure. If the failure process always involves these highly non-linear mechanisms, how is it that a simple linear-elastic theory such as LEFM can be used? This is a question that theoreticians have struggled with for some time. The justification for using LEFM is generally explained as follows: provided the non-linear zone is small compared to the dimensions of the body, that is provided the surrounding linear-elastic zone is much larger than the process zone, then conditions of stress and strain inside the non-linear zone, though they may be poorly known, are nevertheless uniquely characterized by conditions within the linear zone. This statement is much easier to make than it is to prove, for the interested reader. Broberg, in his recent book, probably comes closest to a theoretical proof (Broberg, 1999). Most readers will be more convinced by the experimental evidence which shows overwhelmingly that, provided this so-called `small-scale yielding' criterion is obeyed, the brittle fracture strength and HCF strength of specimens containing cracks can be accurately predicted using the

stress-intensity parameter, K. There are, in addition, some other limitations to the successful use of LEFM, for example the crack length must also be large compared to the plastic zone size. These issues are covered in detailed testing standards which have been developed by various national and international bodies.

In addition to the processes which occur in front of the crack tip, some mechanisms operate behind the crack tip, in the region which is referred to as the crack wake. Here we find the remains of the crack-tip plastic zone, in which there are often significant residual stresses. These residual stresses can affect subsequent crack propagation, especially in fatigue where they alter the level of crack closure. In materials which do not display much plasticity there are a variety of crack-wake mechanisms which may act to improve toughness, such as bridging of the crack faces by fibers or unbroken ligaments of material. Given the little space develop, this is one reason why short cracks, may show different behavior from long cracks.

Elastic-plastic fracture mechanics

The most unfortunate thing about LEFM is that it cannot be applied to many of the practical situations for which we would really like to use it, to predict fracture in components made from tough materials such as metals and composites. Most components made from these materials sustain large zones of plasticity or damage before failure, thus violating the small-scale yielding criterion. Notable exceptions are ferritic steels at low temperatures which fail by cleavage at low stress intensity, and some structures in which exceptionally long cracks may occur, such as pressure vessels or pipelines.

This problem has been addressed by the development of modified forms of fracture mechanics. These innovations have occurred particularly in relation to metallic materials, where they are known by the general heading of elastic-plastic fracture

mechanics (EPFM). A number of parameters have been developed to replace K, notably the crack-opening displacement δ and the J integral. A particular problem here is that, when the conditions for LEFM are violated, this is often accompanied by a change in fracture mechanism. For example, brittle fracture, which classically involves sudden, unstable crack propagation, may, under conditions of increased plasticity, change into a process of gradual, stable crack extension, the amount of crack growth gradually increasing with applied load. This stable crack growth may continue indefinitely, or may become unstable at some critical load. In some cases the location of cracking may shift from the main crack to the center of the specimen, where higher levels of constraint occur. Regarding the mechanics of the situation, the presence of large-scale yielding usually implies a loss of local control of the fracture process, so that the nature of the external loading (for example, whether the body is under load control or displacement control) will now have an effect.

Finite Element Analysis

The last few decades have seen an enormous rise in computing power and, with it, methods of numerical analysis which allow us to simulate complex systems. This has had a profound effect on engineering design. Today, techniques to estimate the forces and stresses in components such as multi-body analysis and FEA are available to designers even in relatively small engineering companies. This means a qualitative change in the way in which components are being designed, as we move away from simplified analytical calculations and empirical rules towards computer simulations.

The same changes are being witnessed in many other fields of science and engineering. A good example is weather forecasting, where systems which are so complex that analytical solutions will never be possible can now be tackled using large computer models. These developments have naturally brought about

corresponding changes in the way in which research is being conducted. It now becomes more relevant to study those kinds of theoretical approaches which can be incorporated into computer models rather approaches based on the solution of analytical expressions, though the latter will always be of value at a scientific level.

A computer model will only ever be as accurate as our knowledge of its boundary conditions, such as the applied loads and restraints. FEA still has some important limitations with regard to the size and complexity of components that can be modeled, especially when using accurate material descriptions incorporating non-linear and anisotropic behavior. However, the critical distance methods described in this work require only linear-elastic stress analyses. For many engineering components the necessary stress-distance data can already be obtained using the kinds of FE model already employed routinely in engineering companies.

Limitations and Challenges in Failure Prediction

In this first part we have described, in summary, the state of the art in the prediction of material failure as articulated in national standards and specifications and as it is used in practice in engineering companies. The current position is unsatisfactory, containing limitations which ultimately affect our ability to design load-bearing structures with confidence.

We can predict material failure with precision only in two rather special cases. The first is simple tension, as described by the stress-strain curve, and the second is the propagation of pre-existing cracks as described by LEFM. The tensile test is of limited practical value because conditions of pure tension arise only rarely in real components. In fact, the strength of the material as measured in a tensile test (σ_u) can often be misleading. Ductile materials fail in a tensile test by a process of plastic instability (necking) which does not occur in other types of loading such as bending

or tension, and the tensile strength of brittle materials is usually determined by small pre-existing flaws, the size of which will depend on processing parameters and specimen size. The LEFM, as we have seen, is a wonderful tool in those cases where it is applicable, but more often than not, when we want to use it, we find that it is not applicable. As regards brittle fracture occurring under constant or monotonically increasing loads, LEFM can only be used for components which contain pre-existing cracks of sufficient length, in components which are sufficiently large to maintain the small-scale yielding criterion. This effectively rules out many components of moderate size, made from relatively tough materials. As regards cyclic loading, LEFM finds an important application, probably its most important practical use, in the assessment of fatigue cracks in critical structures such as aircraft, offshore structures and chemical plant. Due to this, its applications are limited to those components which can sustain relatively large cracks before failure (usually of the order of centimeters) and in which regular inspection procedures can be used to monitor the growth of the cracks over long periods of time. For this reason, LEFM is of very limited value, for example in, car components or other mass-produced consumer products.

Experimental campaign

As the analysis of the resistance of parts and structural elements whit notches, there are various theoretical approaches that provide good results. However, to obtain correct analytical results, the behavior must be linear elastic (or small scale yielding) and must be subjected to a stress in mode I, II or mixed mode (for the stress in mode III, currently there are few results). Not all materials have a linear elastic behavior, except the structural materials in which it is usual to seek certain levels of ductility in order to prevent catastrophic failure. Therefore, a first requirement that has been researched in the material is that such material leaves the linear elastic behavior. Nevertheless, since the rupture in the presence of notches or defects for ductile materials has been little investigated, a material with a behavior not so different from the linear elastic has been chosen. For this reason, a material which presents a macroscopically brittle fracture, but also a behavior that deviates from linearity, has been taken in consideration this type of material is also call quasi-brittle. The experimental campaign has focused on Mode I and Mixed Mode.

Material chosen

The material must have a certain non-linearity behavior, however it must break with brittle mechanisms, avoiding ductile breaking (which are much more complex). These tests method cover determination about failure load of ballistic steel ASTM E-1820, with extremely high yield strength and poor fracture toughness in contrast. This lack of toughness generally involves low damage tolerance and entails a risk to the structural integrity that should be evaluated. When damage consists of the existence of cracks weakening a structural member made from these steels, the

remaining bearing capacity can be predicted by means of well-known Fracture Mechanics theories, but there is no equivalent method to predict the failure load of members containing notches. This work explores the cohesive zone model and the strain energy density model as a tool to predict failure load in such cases.

The stress-strain curve shown in the following figure was obtained as explained in appendix C. The mechanical properties obtained from the stress-strain curve are given in Table 1. This table also includes the fracture toughness of the steel, measured according to ASTM E 399 standard by using fatigue pre-cracked bend specimens 12.5 mm thick.

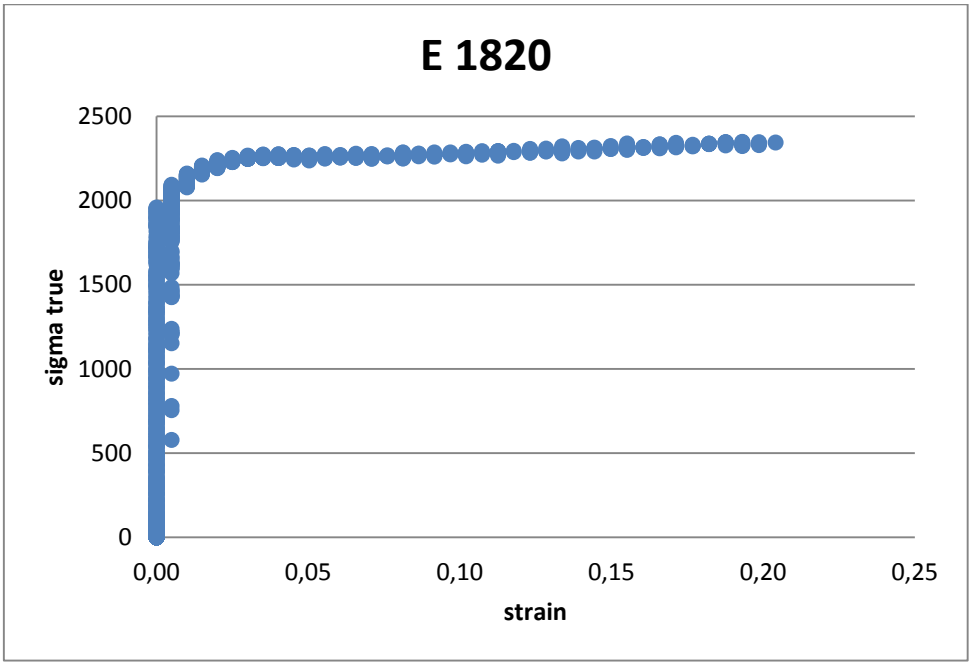

Figura 4 E-1820

Material proprieties:

Mass density	7.85 Kg/dm^3
Elastic modulus	210 GPa
Shear modulus	87.5 GPa
Poisson's ratio	0.2
Fracture toughness	40 MPa m$^{0.5}$
Tensile yield stress	1700 MPa
Failure tensile strength	2100 MPa

Tabella 1 E-1820 Material propierties

Some tests for the determination of fracture toughness have been made. The result that has been obtained is similar to the value used for the simulations (shown in Appendix A).

Specimens used in the experimental campaign

Any analysis that is wanted to run to simulate the behaviour of a material requires an accurate knowledge of the properties of such material. Some of these mechanical characteristics are desired to be validated through experimental tests in order to obtain a more precise definition of the input data which will allow a better accuracy

of the results in output. Regarding this series of test the fracture toughness has been certificated (see Appendix A) but for the definition of material not entirely: an experimental campaign has been conducted but for time reasons, some specimens were not tested. The results that have been obtained are explained in Appendix C.

In this study, the tests are carried out on notched specimens under Mode 1 and Mixed Mode loading. The main objective is to study failure criteria that can predict the failure load for notched specimens with different tip radius. Therefore, this experimental campaign was performed on U-notch specimens with different tip radii of curvature, in order to study the effect of concentration of the tensions caused by different radii of curvature. Figure 5 shows the geometry that has been chosen for both tests:

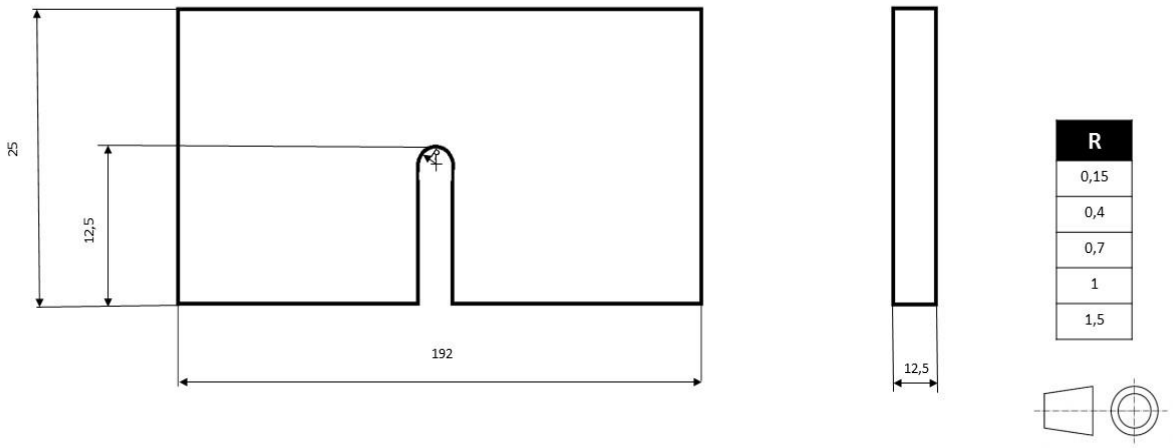

Figura 5 Specimen design

The measures are all in mm. In the tests 5 different tip radiuses have been used. The extent of the specimens is 192mm and the U-notch should be in the middle. The material was purchased in bars; each bar was cut and afterwards the U-notch has been

made with an Electrical discharge machining (EDM). In the EDM the material is removed from the work piece by a series of rapidly recurring current discharges between two electrodes, separated by a dielectric liquid and subject to an electric voltage. With this technique it is possible to obtain small tip radius. Before the tests started the real tip radius of every specimen has been certificated, in Appendix B it is possible to verify the procedure that has been followed. For a good correlation between nominal radius and real one, it has been chosen to considerate the nominal tip radius for the simulation part.

Experimental equipment

The tests have been conducted in the lab of Departamento de Ciencia de Materiales, E.T.S.I. de Caminos, Canales y Puertos, Universidad Politécnica de Madrid (UPM).

To test, an INSTRON machine has been used, model 8803 a hydraulic machine. In static tests the machine can provide a force of 50kN while in dynamic tests 25kN. An important difference between the hydraulic and electromechanical machines is that the first during the movements can be more fast, so a particular attention during the test is required.

In order to eliminate torsional action on the specimen, the loading block and one of the supports should be rotatable around their axes in the direction coincidental with the specimen axis. Both supports shall be hinged supports having rollers. The supports shall be horizontally movable to avoid any restraint on the deformation until the specimen completely ruptures

Figura 6 INSTRON machine, model 8803

This machine could work in load or displacement control. In addition to load and displacement the output of the machine, there could be used two different strains extensometers. In our case we used only one extensometer. The control system is visible in the following picture:

Figura 7 Control system

The extensometer that has been used for checking the specimen is a MTS model 632.03C-51 with a base length of 12.5mm ±2.5 and an error at full scale lower of 0.5%. The extensometer has been used because we want to check the crack mouth opening displacement (CMOD). This choice has been made because we use a quasi-brittle material, and the crack propagation is extremely fast. With this type of material if we try to plot load versus displacement the graphic could be inaccurate in the part of crack propagation, but if we plot load versus CMOD the result is more accurate. Furthermore the displacement is less accurate because there could be shifts of specimen.

Figura 8 MTS model 632.03C-51

The CMOD should be measured using a clip gauge that is capable of measuring the complete rupture of the specimen. After the extensometer has been calibrated, it has been fixed under the specimen using glue for can read the crack mouth opening displacement.

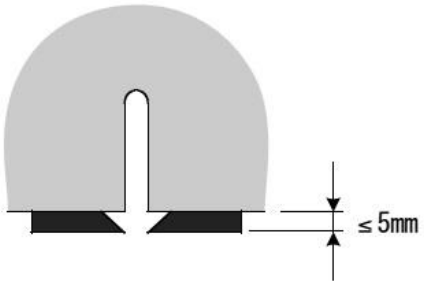

Figura 9 Clasps for extensometer

Before the test starts the machine should be given an auto tuning a stage when the system has been enabled the correction of an out-of-tune performance. All the parts are connected to the computer and the program Easy DAQ v.3.2 reads and saves the output and converts the input from Volt to mm or MPa.

Figura 10 Easy DAQ v.3.2 program

In the tests under Mixed Mode, have not been possible uses an extensometer because there was not space for attack the clip so we have decided to use a camera. The camera used a Vic 3D used like a laser extensimeter. To make this work intense and constant light, so we have used two lamps were used for the light in order to avoid variations of intensity the machine has been surrounded by panels. The camera was connected to computer and for capture and analyse the picture used the program Vic Snap LSE298-03 has used to capture and analyse the picture.

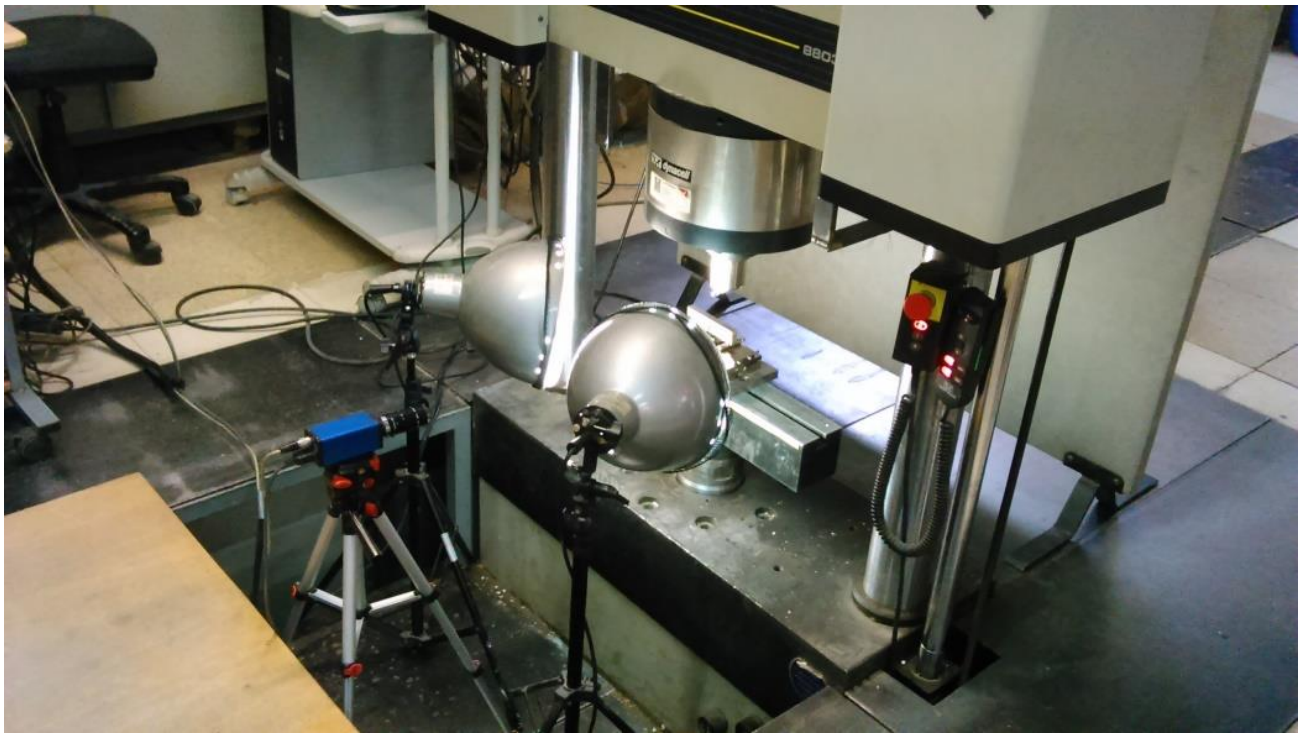

Figura 11 Configuration for mixed mode tests

We could not use the simple specimens because the program needed to identify points in the figure. Every specimen has been painted with a base of withe and after using a spray a lot of black points have been shown in the specimen. Once the test was ended, the program was able to use these points like an extensometer. In the figure 12 is possible to see an example of a painting specimen:

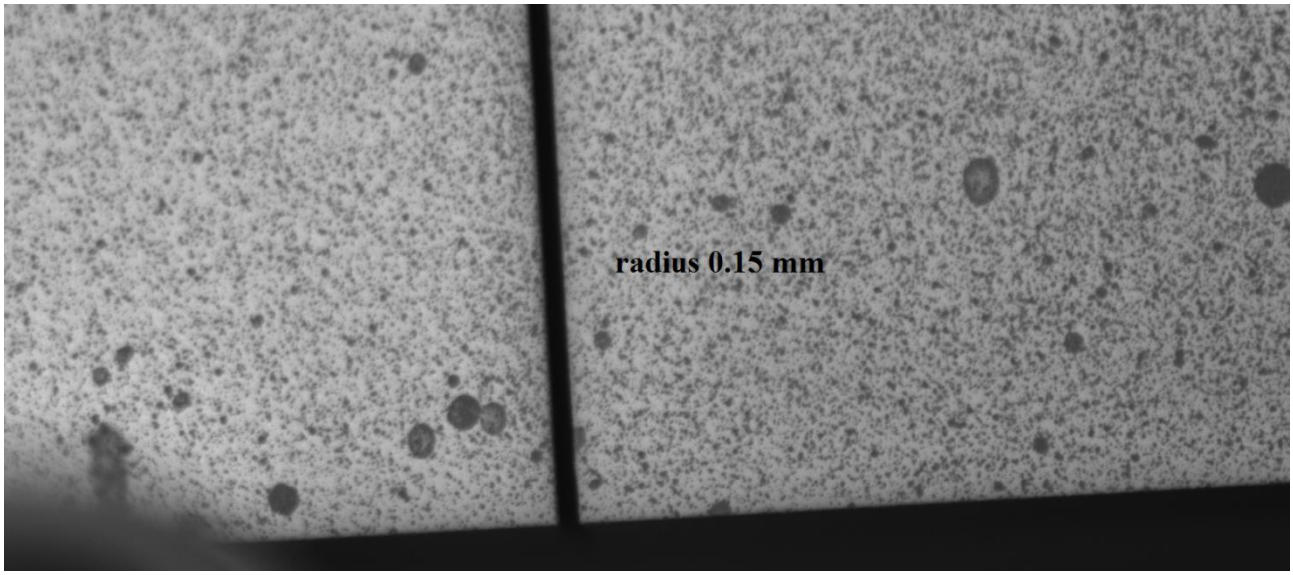

Figura 12 Points used in mixed mode specimens

Mode I tests

The mode I is also called opening Mode. In Mode I the direction of the load is normal to the direction of the crack. Therefore, in the other mode Irwin proposes a series of equations to describe the tension field in a limited zone in front of the crack tip. These equations are written in a Cartesian coordinate system. Also the normal tension is reported, in the plane stress case and plane strain case (normally plane strain case is used like in our case). The Irwin equation for Mode I (see figure 1):

$$\sigma_x = \frac{K_I}{\sqrt{2\pi r}}\cos\frac{\theta}{2}\left(1 - \sin\frac{\theta}{2}\sin\frac{3\theta}{2}\right)$$

$$\sigma_y = \frac{K_I}{\sqrt{2\pi r}}\cos\frac{\theta}{2}\left(1 + \sin\frac{\theta}{2}\sin\frac{3\theta}{2}\right)$$

$$\tau_{xy} = \frac{K_I}{\sqrt{2\pi r}}\sin\frac{\theta}{2}\cos\frac{\theta}{2}\cos\frac{3\theta}{2}$$

The stress component perpendicular to the plane is:

- in plane stress case: $\sigma_z = 0;$

- in plane strain case: $\sigma_z = \nu(\sigma_x + \sigma_y) = 2\nu \frac{K_I}{\sqrt{2\pi r}} \cos\frac{\theta}{2};$

The value of the out of the plane shear stress component is:

$$\begin{cases} \tau_{xz} = 0 \\ \tau_{yz} = 0 \end{cases}$$

In our test three point bending test (TPB) was developed.

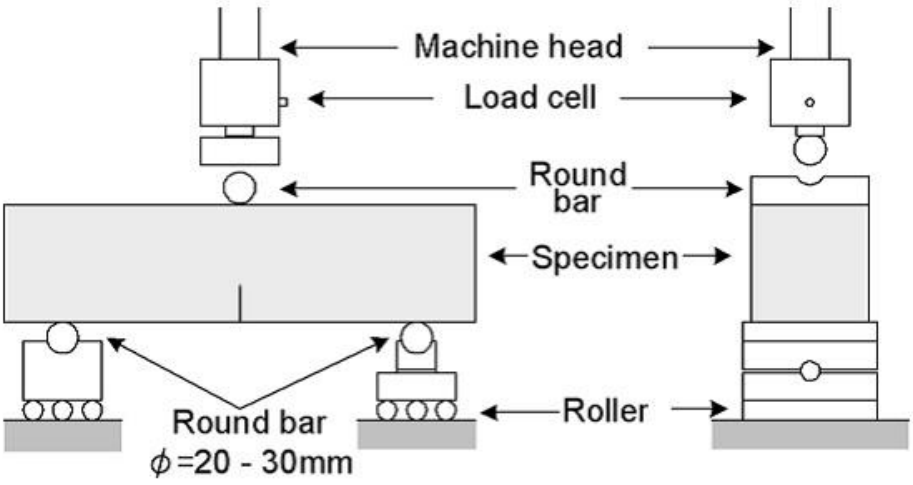

Figura 13 TPB schema

The span between supports is 100 mm. After that the specimen has been put in position and the machine has been placed in a displacement control. This type of control has been preferred to a load control because it is more safe and easier to manage for the machine itself. In our case we have chosen a displacement rate of 0.3 mm/sec. For safety reasons, some limits must be imposed, we have imposed a limit on position; so that when machine when arrives to a precise point, it stops. Therefore we avoid risking to damage the machine.

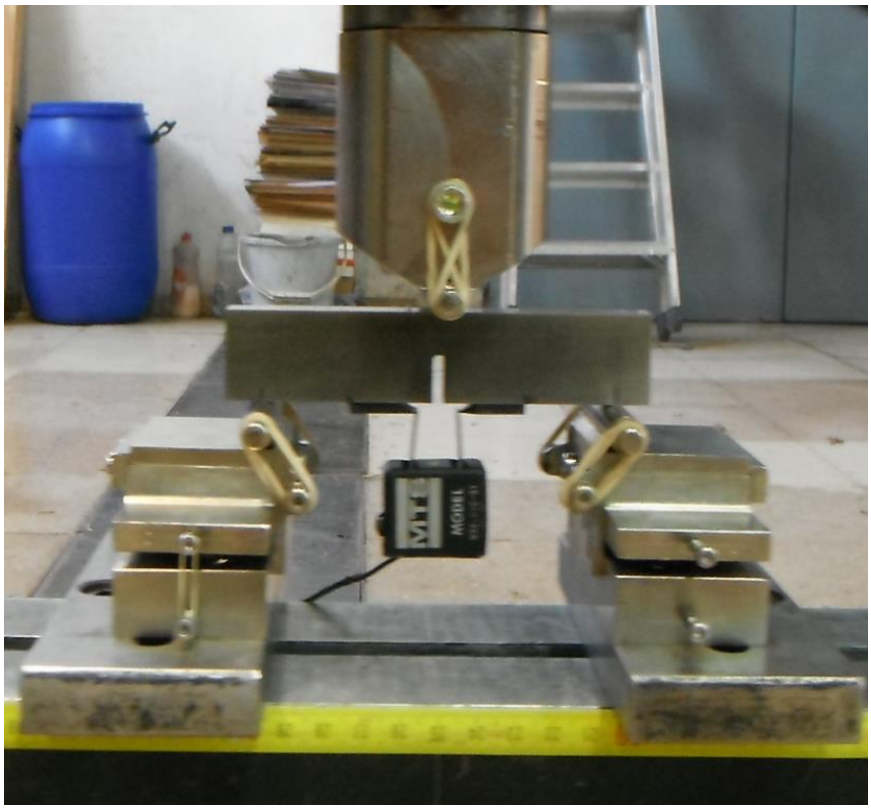

Figura 14 Mode I test photo

In the following table, the results of failure load have been written. In the case of the specimens with tip radius of 1.5 mm there are two anomalous results, maybe caused by a defect in the specimens. Because of this, for the next considerations these two results have not been considered.

Radius [mm]	Failure load [N]	Probeta name
1,5	40240	I
1,5	27000	II
1,5	42264,8	III
0,15	22379,5	IV
1	38000	V
1	40000	VI
1	36220	VII
0,7	31890	VIII
0,7	37560	IX
0,7	36260	X
0,15	22000	XI
0,15	22910	XII
0,4	32240	XIII
0,4	28560	XIV
0,4	31210	XV
1,5	26600	XXI
1,5	35430	XXII

Tabella 2 Experimental failure load Mode I

For every test that we have made, we have calculated every moment: time, load, displacement and CMOD. If we try to plot the graph, for example load versus displacement, we see that the result is similar to our expectations. For instance in the following figure we report the graph load versus displacement for specimen V:

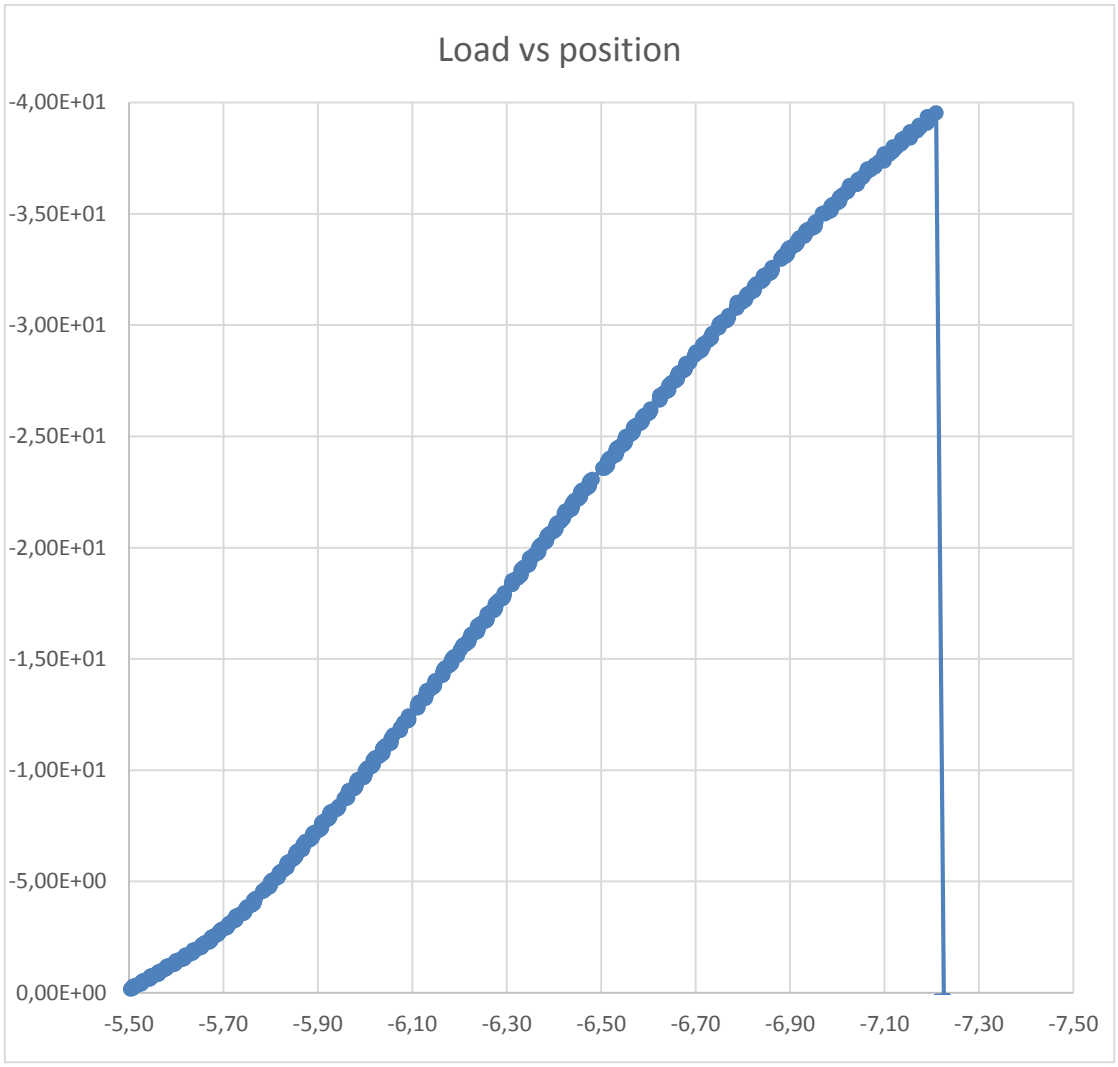

Figura 15 Load vs position Mode I test

Report the relationship between failure load and tip radius could be interesting. We see that the results are included in a band:

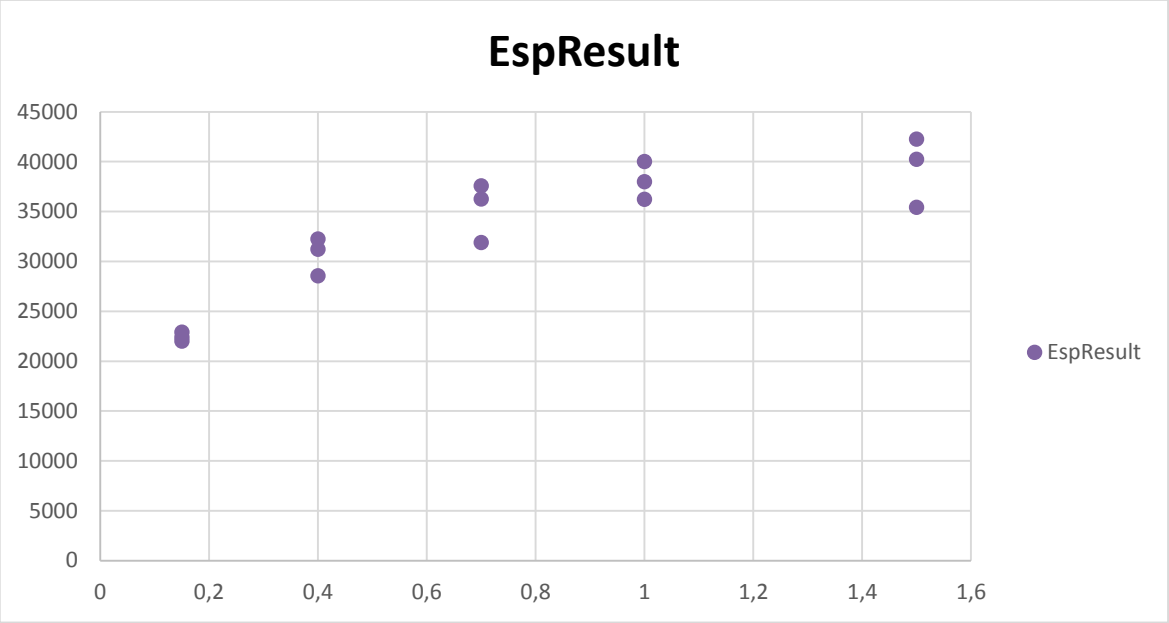

Figura 16 Experimental results Mode I

These results are reasonable. The crack should start in the higher part of the U-notch where we expect to have the grater stress concentration. If we analyse the specimens we see that they have followed this behaviour with the exception of the specimens with a tip radius of 1.5 mm. In these specimens the crack does not start at the tip but near it.

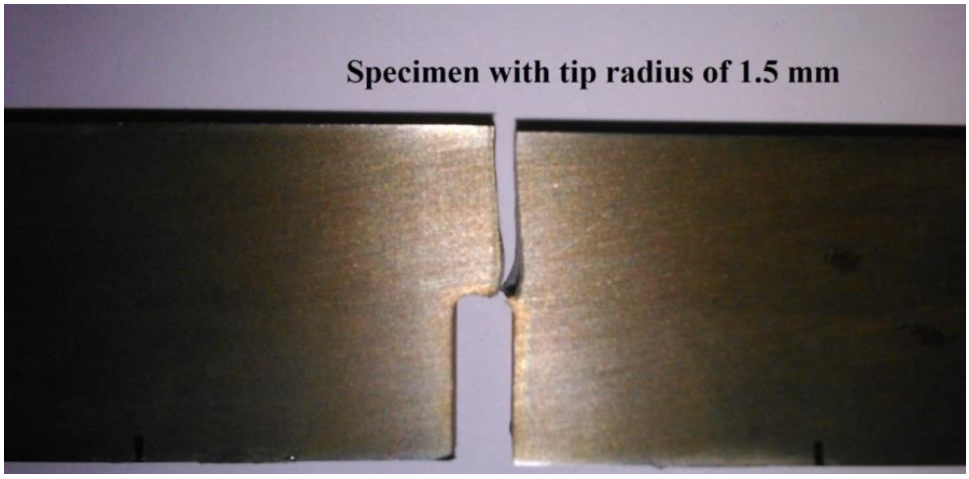

Figura 17 Radius 1.5mm broken specimen

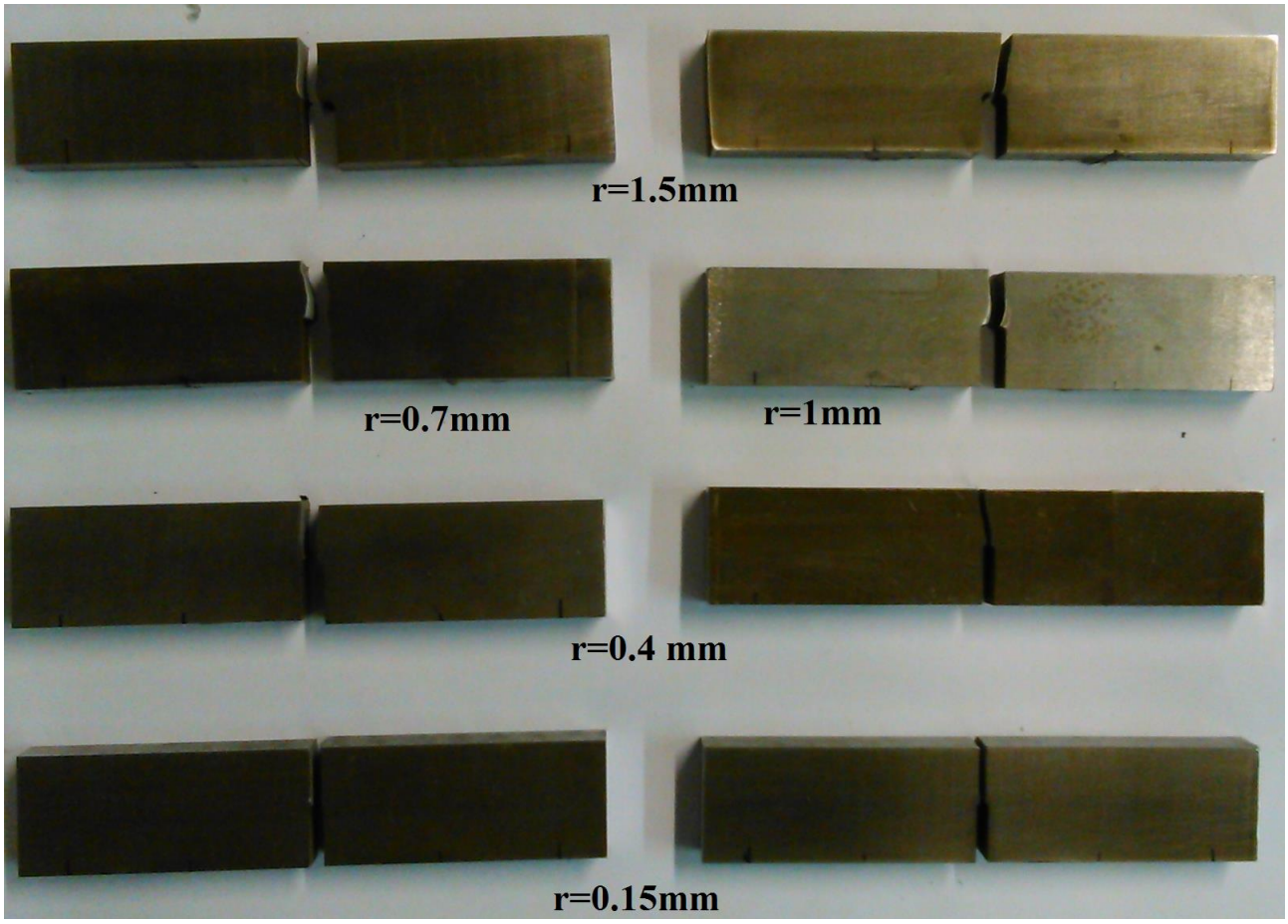

Figura 18 Mode I broken specimens

The figure shows that, with a tip radius different from 1.5 mm the crack starts in the tip of U-notch.

Mixed Mode tests

These tests have been made in mode mixed, in our case the tests have been made with a combination of Mode I and Mode II. The equations developed for Mode I have been explained in the previous section. Mode II also called Sliding mode, is the model in which a shear stress act parallel to the plane of the crack and perpendicular to the crack front.

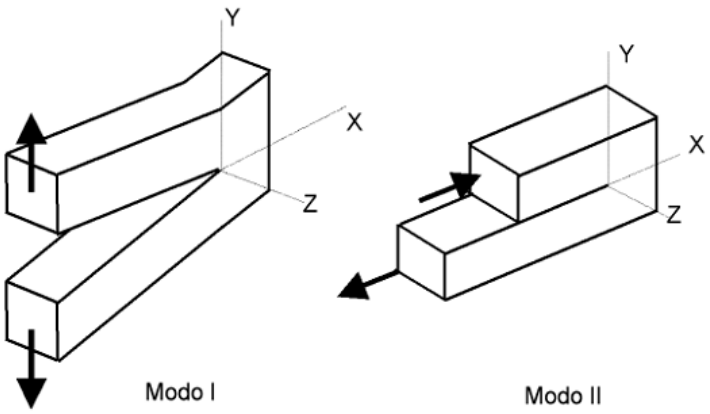

Figura 19 Mode I and Mode II

As in Mode I also in Mode II Irwin proposes a series of equations to describe the tension field in a limited zone in front of the crack tip. Those equations are reported and, written in a Cartesian coordinate system. The normal tension is reported in the plane stress case and plane strain case (normally plane strain case is used). The Irwin equation for Mode II (see figure 1 for references) is as following:

$$\sigma_x = \frac{K_{II}}{\sqrt{2\pi r}} \operatorname{sen}\frac{\theta}{2}\left(2 + \cos\frac{\theta}{2}\sin\frac{3\theta}{2}\right)$$

$$\sigma_y = \frac{K_{II}}{\sqrt{2\pi r}} \sin\frac{\theta}{2}\cos\frac{\theta}{2}\cos\frac{3\theta}{2}$$

$$\tau_{xy} = \frac{K_{II}}{\sqrt{2\pi r}} \cos\frac{\theta}{2}\left(1 - \sin\frac{\theta}{2}\sin\frac{3\theta}{2}\right)$$

The stress component perpendicular to the plane is:

- in plane stress case: $\sigma_z = 0;$
- in plane strain case: $\sigma_z = \nu(\sigma_x + \sigma_y);$

The value of the outside of the plane shear stress component is:

$$\begin{cases} \tau_{xz} = 0 \\ \tau_{yz} = 0 \end{cases}$$

In our case the tests were a mixed mode: a combination of mode I and mode II. A three point bending test (TPB) have been realized. The geometrical definitions are explained in the following figure:

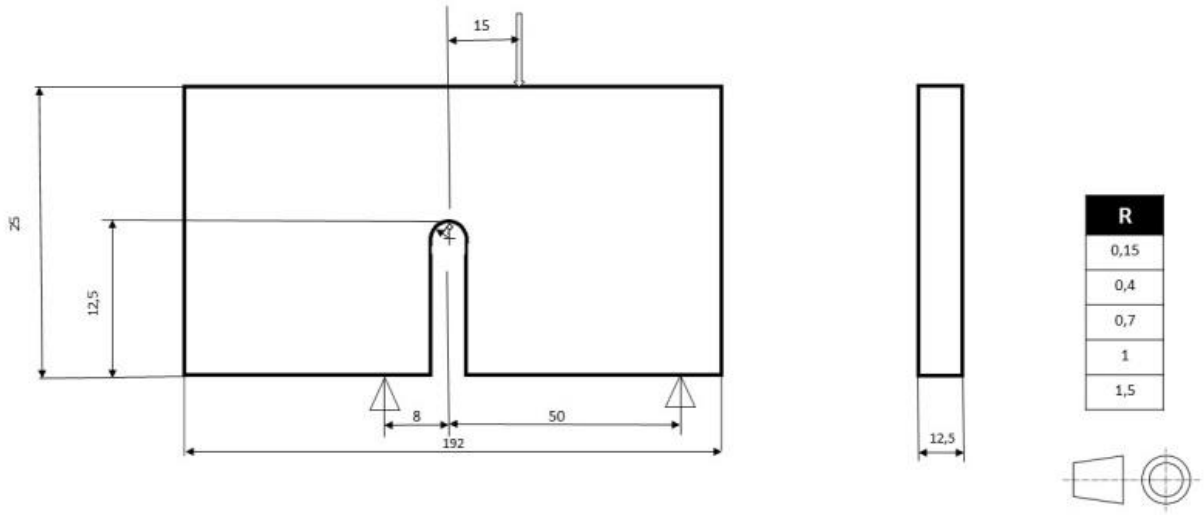

Figura 20 Mixed Mode schema

The specimens have been prepared as it has been explained previously, for making possible the use of the camera. After that it has been put in position and the machine has been put in displacement control. In our case we have chosen a displacement rate of 0.3 mm/sec. For safety reason some limits must be imposed, a limit on position has been set, so the machine when arrive to a precise point stops for avoid risk of damage to the machine.

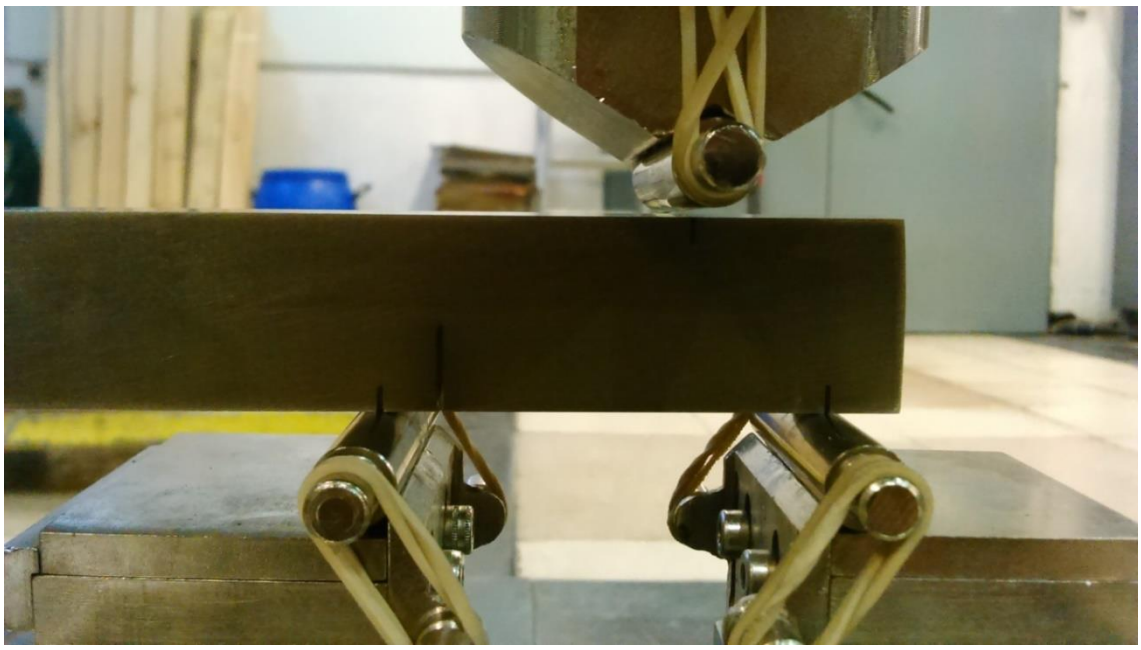

Figura 21 Mixed mode photo

In the following table, the results of failure load have been displayed. The results of specimen XXIII have not been written because the U-notch does not arrive in the middle, therefore the failure load was not comparable with the other results. The specimen XXXII has been used for setting the machine and during this stage it broke without obtaining any results.

Probeta name	Radii [mm]	Failure load [N]
XL	1,5	67651,367
XXXIX	1,5	62433,472
XXXVIII	1,5	71946,716
XXIII	1	
XXIV	1	77067,6
XXV	1	77045
XXVI	1	70226,7

XXIX	0,7	60817
XXX	0,7	76037
XXXI	0,7	57894,3
XXXII	0,4	
XXXIII	0,4	67703,552
XXXIV	0,4	57651,062
XXXV	0,15	61210
XXXVI	0,15	54575,806

Tabella 3 Experimental failure load Mixed Mode

Like in the Mode I tests for every test we have been measured time, load, displacement and CMOD. If we try to plot the graph for example load versus displacement we see that the result is similar to our expectations. For example in the following figure we report the graph load versus displacement for specimen XXX:

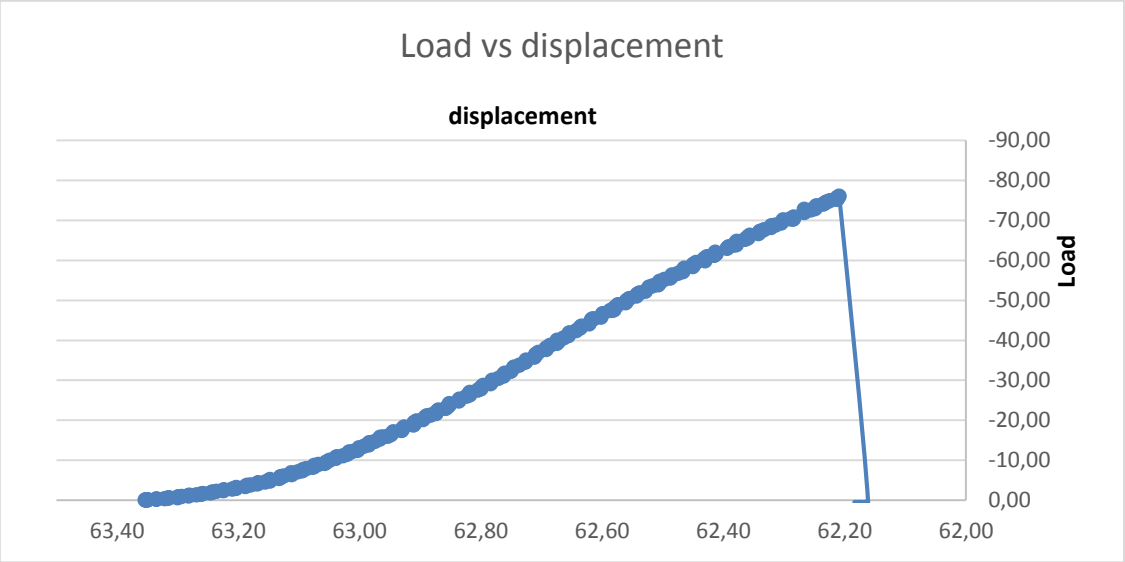

Figura 22 Load vs displacement mixed mode test

Reporting the relationship between failure load and tip radius could be interesting. We see that the results are included in a band:

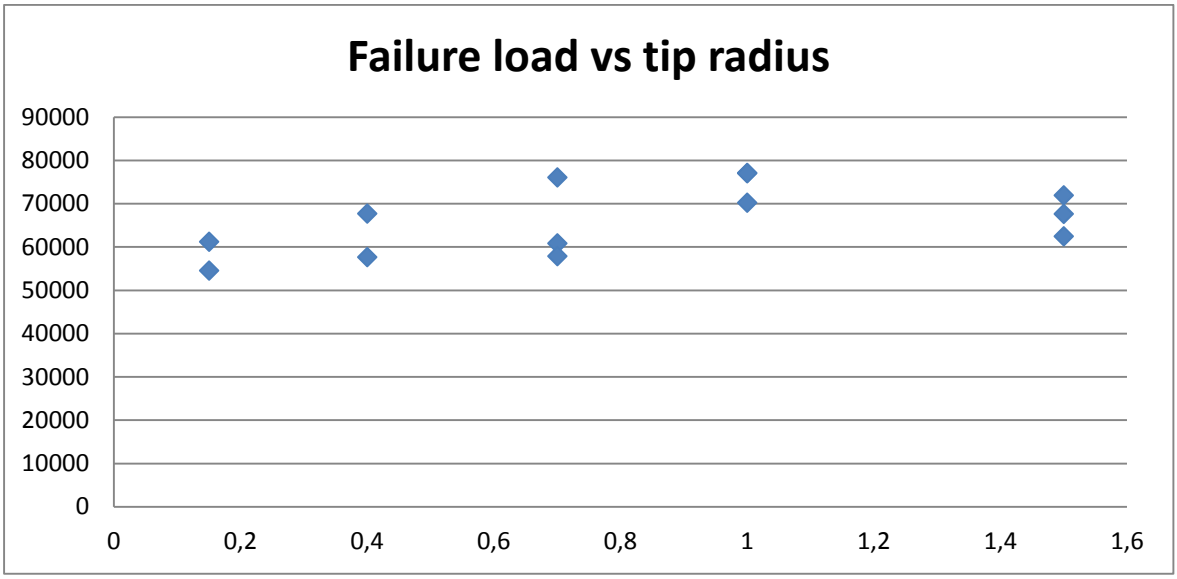

Figura 23 Experimental results Mixed Mode

As we could predict, the failure loads in this case are higher in Mode II respect Mode I. Under a mixed mode loading, the maximum stress is no longer centred on the notch tip, but rather on the point along the edge of the notch. The cracks did not start in the top of tip radius but from a specific point. In our test this point is located on the average of 40° from the top.

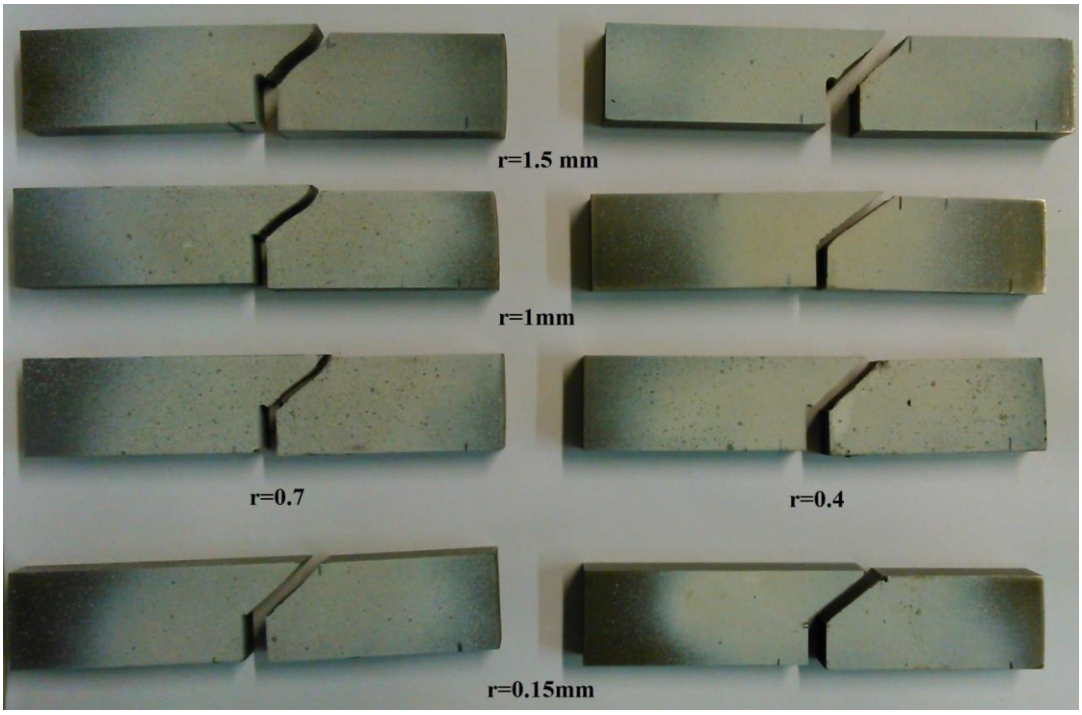

Figura 24 Mode Mixed broken specimens

Numerical Analysis

Cohesive model

The objective of this part is to verify the ability of the numerical model. The verification has been developed in the Department of Materials Science of the Polytechnic University of Madrid, to be able to approximate correctly the behaviour of the material detected experimentally.

The basis of this model are due to Barenblatt (1959, 1962), Dugdale (1960) and Rashid (1968) (Kumar & Barai, 2011). The cohesive crack model, also called fictitious crack model, affirm that after the propagation of a crack in the material, the ability to transfer stress across it, decreases as a function of its opening.

For quasi-brittle materials, the so called standard formulation assumes that the stress-strain behaviour is isotropic linear elastic, and that the initiation criterion is of the Rankine type. Such that the cracking starts at a given point when the maximum principal stress σ_I at that point reaches the tensile strength f_t, and that the crack is oriented perpendicularly to the principal stress direction associated to σ_I. It also postulates the evolution law for monotonic mode I so that the cohesive stress is a unique function of the crack opening which, is monotonically decreasing, and this phenomenon is called the softening curve (although other denominations are also found in the literature, such as stress–crack opening curve or tension-softening curve).

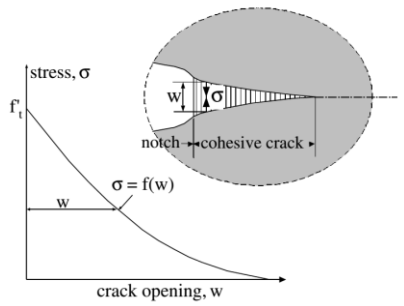

Figura 25 Example of softening curve

The standard formulation has some intrinsic limitations. The most obvious one is that the softening curve is assumed to be a material property, and thus the fracture energy is a constant. Moreover, no energy is dissipated outside the cohesive zone. This is, of course, an approximation, but it has been extensively verified for concrete, and it is expected to do so for other quasi-brittle materials as well. In purity, the softening curve should be expected to depend on triaxiality and maybe also on the relative rotation of the faces of the cohesive crack. However, no specific extensions have been developed to include such effects. Therefore, the applicability of the cohesive crack in the constitutive sense must be experimentally checked for each material family. Put in another way, this simply means that while we propose the model to extend to a wider range of situations (long cracks, short cracks, no cracks at all, . . .), we cannot expect it to hold for any material a priori, we need to verify it by experiment.

For monotonic Mode I opening, the stress transferred, σ is normal to the crack faces and is a unique function of the crack opening *w*.

$$\sigma = f(w)$$

The function f (w) is called softening curve. Two properties of the softening function are worth noting: the cohesive strength σ_t, and the cohesive fracture energy G_F. The cohesive strength σ_t is the stress at which the crack is created and starts to open, i.e.

$$\sigma(0) = \sigma_t$$

According to experimental tests under Mode I, the cohesive strength is more or less two or three times the failure tensile strength. The cohesive fracture energy G_F, is the external energy supply required to create and fully break a unit surface area of the cohesive crack, and it is given by the area under the softening function:

$$G_F = \int_0^{w_c} f(w)\, dw$$

Where w_c is the critical crack opening, after which the cohesive stress becomes zero. The area under the softening function, G_F, can be computed taking into account that the material behaves as linear elastic, this assumption is almost correct because our material is quasi-brittle. With this assumption the fracture energy could be calculate as following:

$$G_F = \frac{K_{IC}^2}{E/(1-\nu^2)}$$

A further parameter, significant for the structural behaviour, is the characteristic length:

$$l_{ch} = \frac{E\, G_F}{\sigma_t^2}$$

This simple formulation of the cohesive crack model is able to capture the main aspects of the fracture of brittle materials, particularly of components with blunted

notches that do not exhibit a pre-crack or singularity. This model can be generalized in different ways as outlined in Elices et al. and in Planas et al.

In this work we have assumed that:

- Fracture toughness K_{IC}=40 MPa $m^{0.5}$;
- Poisson's ratio ν=0.2;
- Elastic Modulus E=210000 MPa;
- Cohesive strength σ_t≈3200 MPa. We obtain:

The cohesive fracture energy is:

$$G_F = \frac{K_{IC}^2}{E/(1-\nu^2)} = \frac{40^2}{210000/(1-0.2^2)} = 0.007314 \approx 0.008\ MPa\ m$$

And the characteristic length is:

$$l_{ch} = \frac{EG_F}{\sigma_t^2} = \frac{210000 * 0.007314}{3200^2} = 0.000149994\ m$$

LS-DYNA

Part of the simulations performed in this project, were analysed by LS-DYNA v. 971, which is an advanced finite elements program, specifically developed for the resolution of complex nonlinear dynamic problems. With its large range of potential uses, it allows the simulation of complex problems and is widely recognized as the leading analysis software for the most advanced applications of engineering. LS-DYNA is a program used in various sectors such as automotive, aerospace, military and bioengineering and it is used to solve problems involving large deformations, sophisticated material models and complex contact conditions. It has the possibility to set the problem in the time domain, it has a wide range of material models and types of elements, as well as to be able to access various solvers, in addition to the explicit one, present within the same code. The advantage that comes from using the LS –DYNA program, in this part of the project, is the lack of convergence problems arising from the large non-linearity of this problem, contrary to what can happen with conventional programs that use implicit formulation. This is possible because LS-DYNA does not need the definition of the static equilibrium of the structure. The precaution that must be taken against this is that the application speed of the load must be controlled to reduce the inertial forces as much as possible. This is because in this type of program, the inertia contributes significantly to the solution. Another disadvantage that occurs using an explicit code is that the temporal integration requires the discretization in very small intervals of time (about 10-5 s - 10-7 s). Therefore, if the test served to simulate the real time of the test, the simulation could be delayed for months. To solve this problem it is possible to apply the load more quickly than in the real test. However, this is possible by checking that the model does not develop too high inertial forces. In order to avoid this problem, in this project, the kinetic energy of the system was maintained, at least two orders of magnitude lower than its internal energy.

Mesh

To create the models and to analyse the results the program Ls-PrePro 4.2(Beta) has been used.

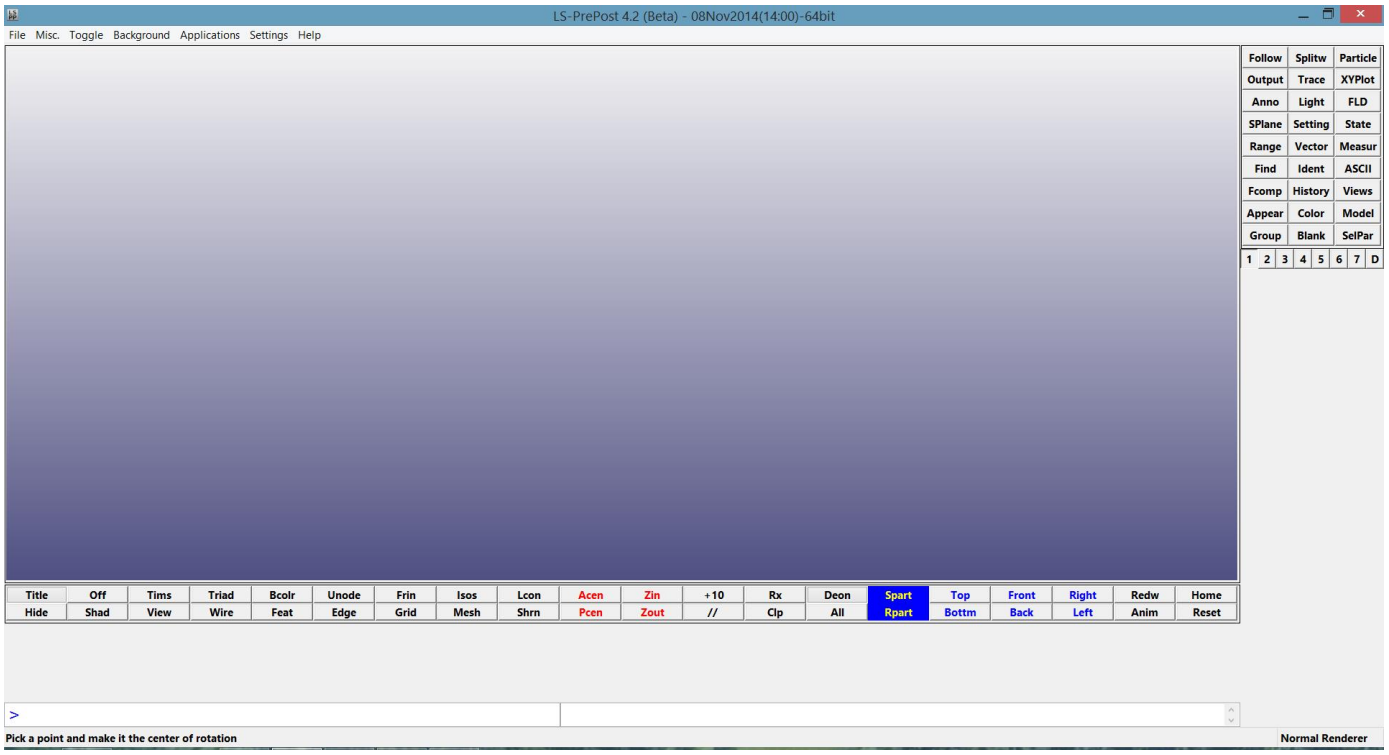

Figura 26 Ls-Dyna

The most important step is the definition of the specimen geometry. The first part is the definition of a two dimensional sketch, after that step the mesh must be created. The dimension of the mesh is inversely proportional with the time to make the simulation. For these reasons the mesh near the notch has been made really dense and far from this area the dimensions of element grow.

In this work we used two different models. The first has been used in the test under Mode I. It plots only half of the specimen because we know the direction of the

crack. In Mixed Model test we do not know where the crack originates and its direction, that is why for these tests all the geometry of the specimens have been used. After that the 2D geometry has been completed, the depth of the specimen must been chosen. To reduce the effect of inertia that contributes the depth has been chosen of 0.1mm.

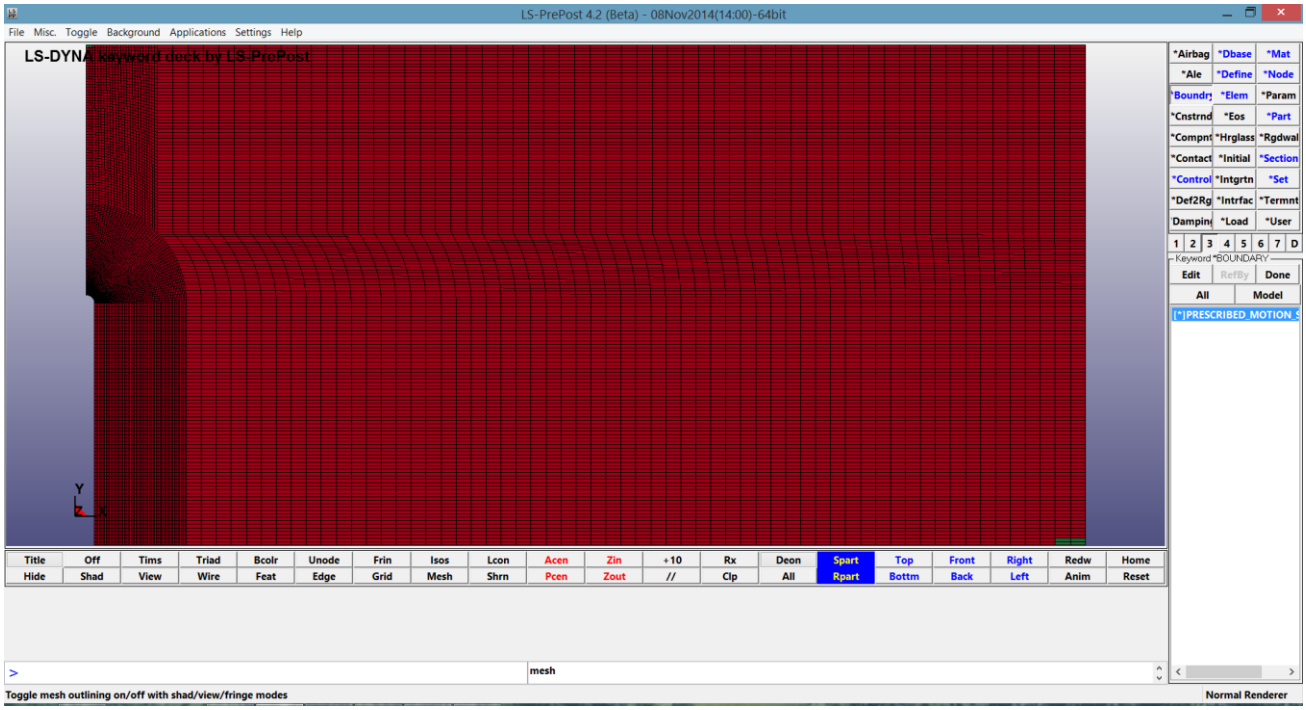

Figura 27 Half specimen mesh

In this first model the symmetry condition is defined in the left part of the model. To define the symmetry condition, the displacement in x direction has been stopped.

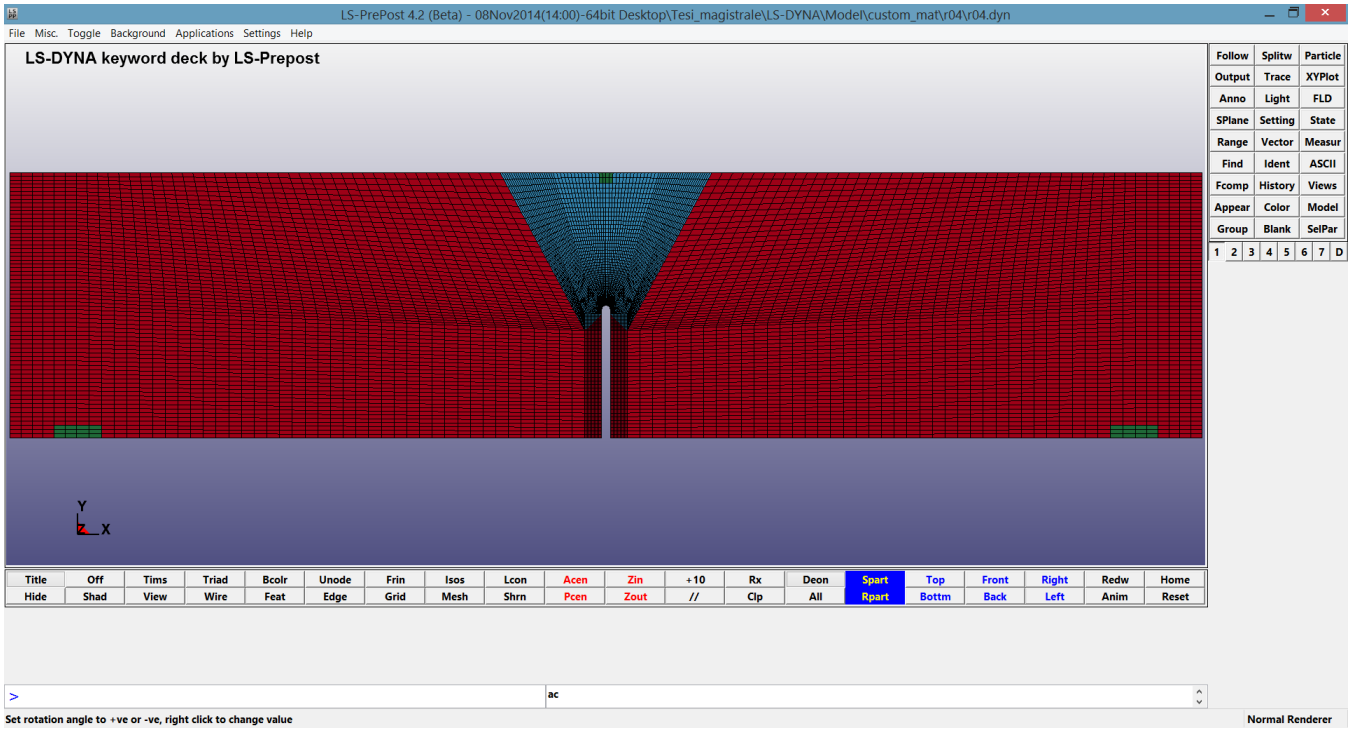

Figura 28 Entire specimen mesh

To complete the model, the restraint condition, the loads, and the type of element must be define. Also the nodes where the conditions are located must be identifying. Regarding the allocation of constraints and loads, in order to simulate correctly the experimental tests, it was decided to impose a state of immobility in the support of the model while a condition of linear load has been imposed. The condition of supports have been imposed with the curve:

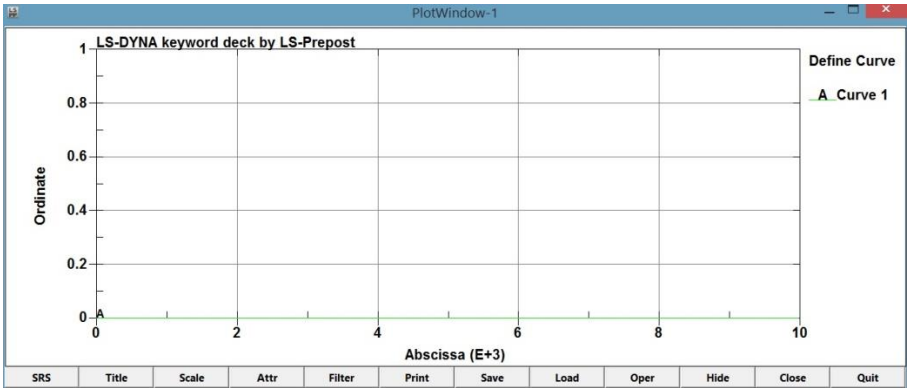

Figura 29 Bond curve

This condition has been imposed also to all elements to stop the displacement in the normal direction to the plane of the specimen face (direction z). While the application of the load has been described with the curve:

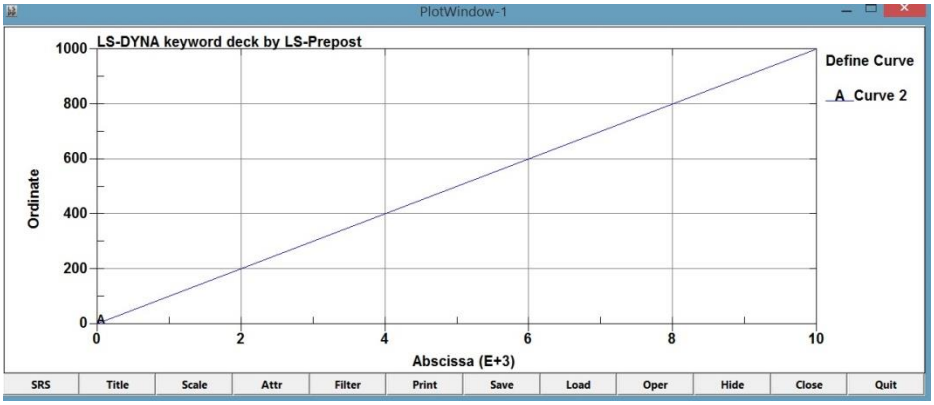

Figura 30 Load curve

Regarding the element type in the model there has been used a different type of element according to the material to which they were associated.

- Element formulation 1

  It is the default element formulation, it is efficient and accurate and it works also for severe deformations, but needs an hourglass stabilization.

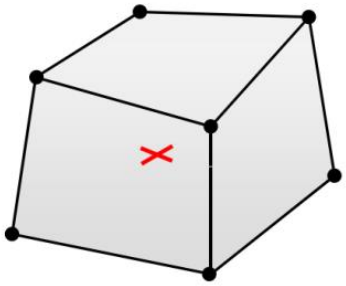

Figura 31 elform 1

- Element formulation 2

  It is slower than element formulation 1 but it does not need a hourglass stabilization. It is too stiff in many situations, especially for poor aspects ratios (shear locking). It is also unstable in large deformations application.

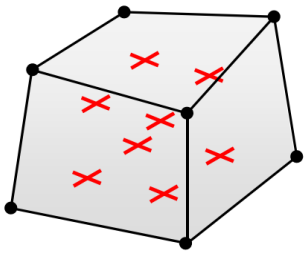

Figura 32 elform 2

- Element formulation 3

  It is a quadratic 8 node hexahedron with nodal, 6 degree of freedom per node. It is well suited for connections to shells. It has a good accuracy for small strains and a tendency to volumetric locking.

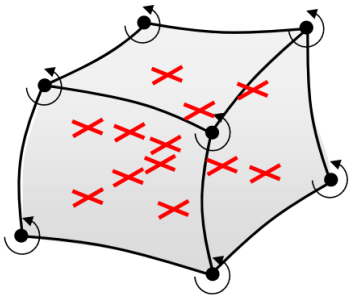

Figura 33 elform 3

- Element formulation 19

  It is a 4 points element. In LS-Dyna only 2 elements can be used with cohesive material models the element formulation 19 and 20. The element formulation 19 is faster than 20 but element 20 will transfer moments between the bonded parts, whereas element formulation 19 will not. A cohesive element can have zero thickness and even invert without becoming unstable.

Materials

Elastic

This material has been used for few elements near the supports and load application points because concentrates forces have been used and problems of indentation could born. For this material the element form 3 has been chosen. This is an isotropic hypo elastic material and it is available for beam, shell, and solid elements in LS-DYNA. The variables of material, further the identification number, are:

- Mass density
- Young's modulus
- Poisson's ratio

This hypo elastic material model may not be stable for finite (large) strains.

Isotropic elastic-plastic

This material has been used for the most part of elements far from the area of propagation of crack. For this material the element form 2 has been chosen. This is a very low cost isotropic plasticity model for three dimensional solids. In the plane stress implementation for shell elements, a one-step radial return approach is used to scale the Cauchy stress tensor to if the state of stress exceeds the yield surface. This

approach to plasticity leads to inaccurate shell thickness updates and stresses after yielding. This is the only model in LS-DYNA for plane stress that does not default to an iterative approach. The variables of material are:

- Mass density;
- Shear modulus;
- Yield stress;
- Plastic hardening modulus;
- Bulk modulus.

Cohesive general

This material type has been used only in tests of Mode I. In these tests we know that the cracks originate in the top of a U-notch, so we have created a series of element in this material along the direction of the crack propagation. This type of material is supported by a limited number of elements formulation, in our case the element formulation 19 has been used. This model includes three general irreversible mixed-mode interaction cohesive formulations with arbitrary normalized traction-separation law given by a load curve. These three formulations are differentiated via the type of effective separation parameter. The interaction between fracture modes I and II is considered, and irreversible conditions are enforced via a damage formulation (unloading/reloading path pointing to/from the origin).

The material variables are:

- Mass density;
- The number of integration points required for the cohesive element to be deleted. If it is zero, the element won't be deleted even if it satisfies the failure criterion. The value of INTFAIL may range from 1 to 4, with 1 the recommended value. We have chosen 1;
- Type of effective separation parameter. We have chosen value 2, that means that a dimensionless separation measure is used, which grasps for the interaction between mode I displacements and mode II displacements;
- Normalized traction-separation load curve, in this part the softening curve must be define;
- Fracture toughness for mode I and mode II (G_I and G_{II});
- Exponent that appears in the power failure criterion. We have chosen 0;
- Peak traction in normal direction (mode I) defines as T;
- Peak traction in tangential direction (mode II) defines as S.

The traction-separation behaviour of this model is mainly given by G_I and T for normal mode I, G_{II} and S for tangential mode II and an arbitrary normalized traction-separation load curve for both modes, the softening curve. The maximum (or failure) separations are then given by:

$$\delta_{failure}^{I} = \frac{G_I}{A\,T}$$

$$\delta_{failure}^{II} = \frac{G_{II}}{A\,S}$$

Where A is the area under the normalized traction-separation curve. The normalized softening curve that we have chosen is:

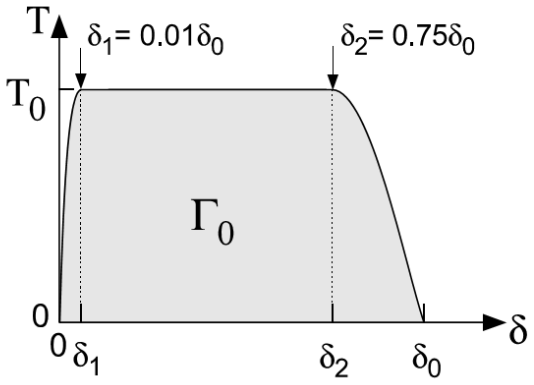

Figura 34 Softening curve chosen

T_0 is 1 like δ_0. The value δ_1 is 1e-10 and δ_2 is 0.9999. In LS-Dyna the curve appears:

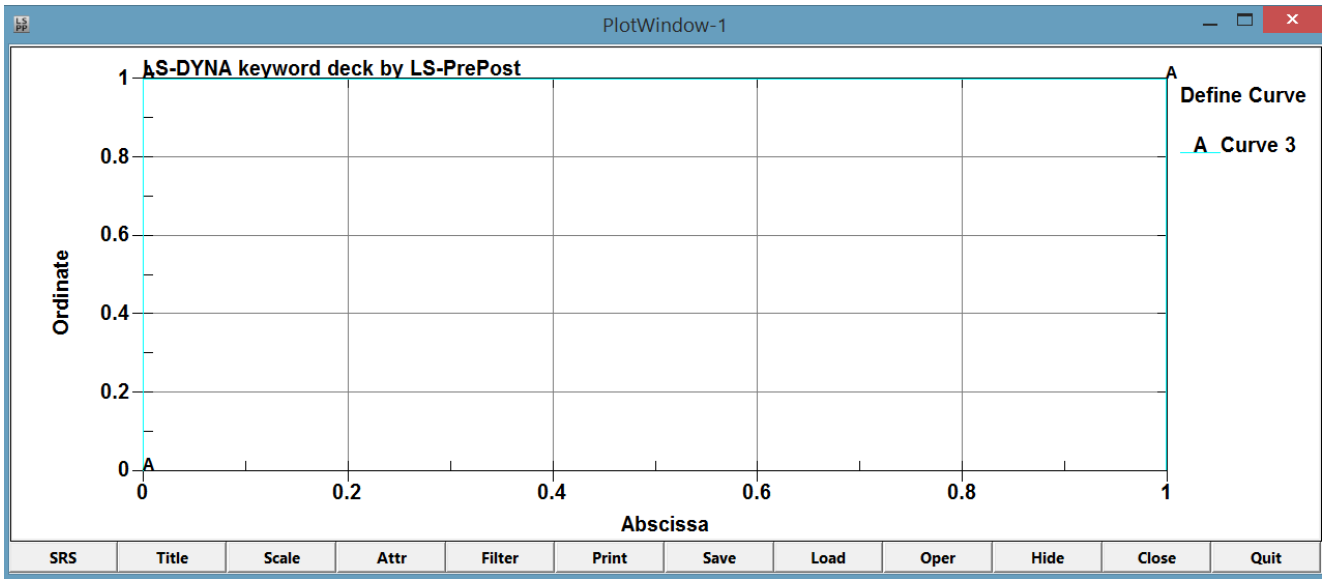

Figura 35 Softening curve used in Ls-Dyna

In this material model a dimensionless effective separation parameter λ is used, which grasps for the interaction between relative displacements in normal (δ_3 mode I) and tangential (δ_1 and δ_2 mode II and mode III) directions:

$$\lambda = \sqrt{\left(\frac{\delta_1}{\delta_{II}^{failure}}\right)^2 + \left(\frac{\delta_2}{\delta_{II}^{failure}}\right)^2 + \langle\frac{\delta_3}{\delta_I^{failure}}\rangle^2}$$

The Mc-Cauley bracket has been used to distinguish between tension ($\delta_3 \geq 0$) and compression ($\delta_3 < 0$). The Mc-Cauley bracket is a notation used to describe the ramp function.

$$\langle x \rangle = \begin{cases} 0; & x < 0 \\ x, & x \geq 0 \end{cases}$$

The values δ_1 and δ_2 are critical values, representing the maximum separations in the interface in normal and tangential direction.

User defined material model

In the tests under mixed mode the points where the cracks originate are difficult to be defined. The cohesive material could be used only if the exact propagation point was known. A material that is not defined in LS-Dyna, has been used and the user must provide a material subroutine.

There are some materials on which failure, although being macroscopically brittle, is preceded by a global nonlinear behaviour. This fact evidences a propagation of the nonlinear regime of the material far beyond the notch tip. Under these conditions, the tools that are available for analysis purposes are scarce, and the use of equivalent linear elastic models is not straightforward because of the difficulties found on identifying the actual energy available for fracture. A model based on the combination of a Hencky's nonlinear material model with a cohesive crack model by using the so called embedded crack approach has been used. Hencky's nonlinear material model is actually a non-linear elastic model that does not dissipate energy during the phases of loading and unloading. For this reason, the simulations will be close to reality only until the material will be subjected only to load cycles, without unload. In this case this is true until the break of the specimen, so it is always true except locally, near the failure condition, where there are some cracks that predominate over the others, discharging them. However this is a minimum contribution that can be neglected.

According to Hencky's material model, the spherical and the deviatoric parts of the stress tensor are obtained separately. The cohesive crack model or fictitious crack model postulates that once a crack is formed in the material, the stress transferring capability across the crack decreases as it is being opened. In a pure mode crack opening I case (crack opening exclusively under tension), the stress transferred across the crack, σ, can be related with the crack opening displacement, w, through the function called softening curve. In a general 3D case, once the crack is formed and its orientation **n** fixed, it should be able to open at any arbitrary direction of the 3D space. Therefore, crack opening must be defined as a vector polar, **w**, instead of a scalar one. To expand the mode I softening curve concept to make it compatible with three dimensional crack openings, a central forces model has been used. According to this model, the traction vector across the crack **t** is parallel to the opening vector **w** and has a magnitude equal to the actual value of the softening curve.

Therefore the traction vector reads:

$$\vec{t} = \frac{f(\widetilde{w})}{\widetilde{w}}\vec{w}$$

Being $\vec{t}$ the traction vector, $\vec{w}$ the crack opening vector, $f(\widetilde{w})$ the softening curve, and $\widetilde{w}$.The Euclidean norm of the crack opening vector.

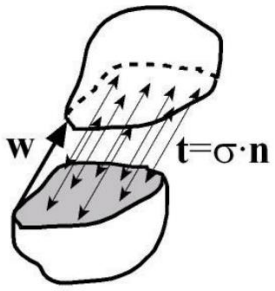

Figura 36

According to the embedded crack approach, once the crack appears inside the element, it modifies the strain field so an apparent strain tensor (without taking into account crack opening) and a continuum strain tensor (subtracting the crack opening) must be distinguished. In the case of a constant stress element, assuming also constant crack opening, the relationship between both strain fields reads:

$$\varepsilon_{cont} = \varepsilon_{app} - \left[\overrightarrow{b^{+}} \otimes \vec{w}\right]^{S}$$

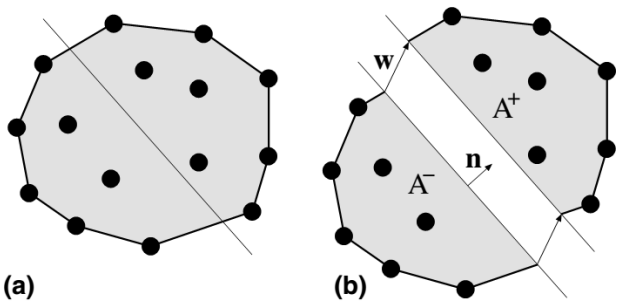

Figura 37

Being $\varepsilon_{cont}\ and\ \varepsilon_{app}$ the continuum and the apparent train tensors respectively, **w** the crack opening vector $\overrightarrow{b^+}$ the vector of gradients of the solitary nodes shape functions:

$$\overrightarrow{b^+} = \sum_{\substack{i=solitary \\ nodes}} gradN_i$$

$$\varepsilon_{app} = \sum_{i=nodes} [gradN_i \otimes u_i]^S$$

The solitary nodes are defined as the set of nodes that are put apart by the crack from the rest of the element. The term u_i represents the approximated nodal displacement. The following figure illustrates the above mentioned concepts:

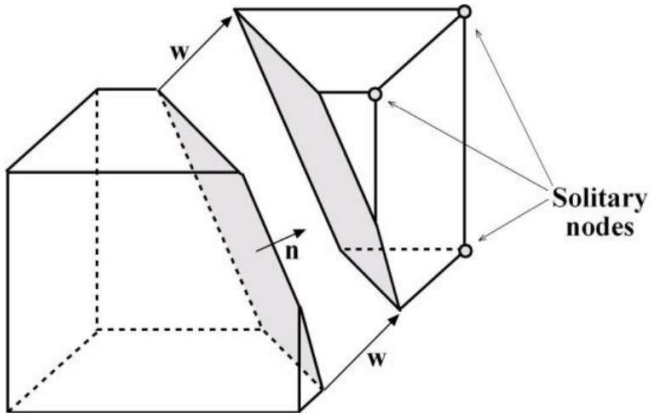

Figura 38

For a given crack direction **n**, there are several possible combinations of solitary nodes. Again following among all the possibilities, in this work we have used the combination that minimizes the angle between $\vec{n}$ and $\overrightarrow{b^+}$.

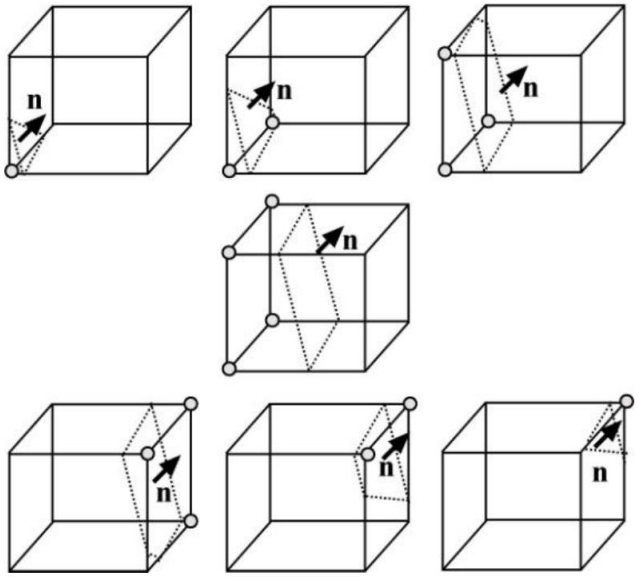

Figura 39

Once the crack is initiated, the vectors $\vec{n}$ and $\overrightarrow{b^+}$ are fixed and as the strain tensor increases, the crack displacement **w** must be obtained. Since in the continuum part the material behaves according to Hencky's constitutive law and across the crack the material behaves according to the softening curve, by prescribing local equilibrium, we could find an equation whose meaning is that the traction vector on the continuum associated to the normal direction **n**, must be equal to the traction transferred across the crack.

Initially **w**=0 in the element $\vec{n}$ and $\overrightarrow{b^+}$ are undefined, thus the load until the maximum principal stress exceeds the tensile strength. Then a crack is introduced perpendicular to the direction of the maximum principal stress, and $\vec{n}$ is computed as a unit eigenvector of **σ.** Next, the solitary node and the vector $\overrightarrow{b^+}$ are determined by requiring that the angle between $\vec{n}$ and $\overrightarrow{b^+}$ be the smallest possible. This is

equivalent to selecting the solitary node so that the side opposite to it is as parallel as possible to the crack. This procedure was devised based on the observation of Borja that the behaviour of this type of element is best when the crack meets such condition, and also based on the analysis in the previous section showing that the local and global equilibrium are simultaneously met only when $\vec{n}$ is parallel to $\overrightarrow{b^+}$.

This procedure is carried out at the element level, and is strictly local: no crack continuity is enforced or crack exclusion zone defined. This leads in many circumstances to locking after a certain crack growth. Such locking seems to be due to a bad prediction of the cracking direction in the element ahead of the pre-existing crack, as sketched in the following figure although in our element shape is a quadrangle:

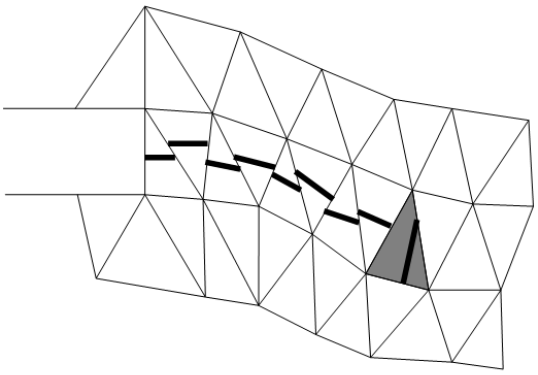

Figura 40

To overcome this problem without introducing global algorithms (which could make the system very complex and slow), we have introduced a certain amount of crack adaptability within each element. The rationale behind the method is that the estimation of the principal directions in an element is especially bad at crack initiation due to the high stress gradients in the crack tip zone where the new cracked element is usually located; after the crack grows further, the estimation of the principal stress directions usually improves substantially.

Therefore we allow the crack to adapt itself to the later variations in principal stress direction while its opening is small. This crack adaptation is implemented very easily by stating that while the equivalent crack opening at any particular element is less than a threshold value $\widetilde{w}_{th}$, the crack direction is recomputed at each step as if the crack were freshly created. After that $\widetilde{w} > \widetilde{w}_{th}$, no further adaptation is allowed and the crack direction becomes fixed.

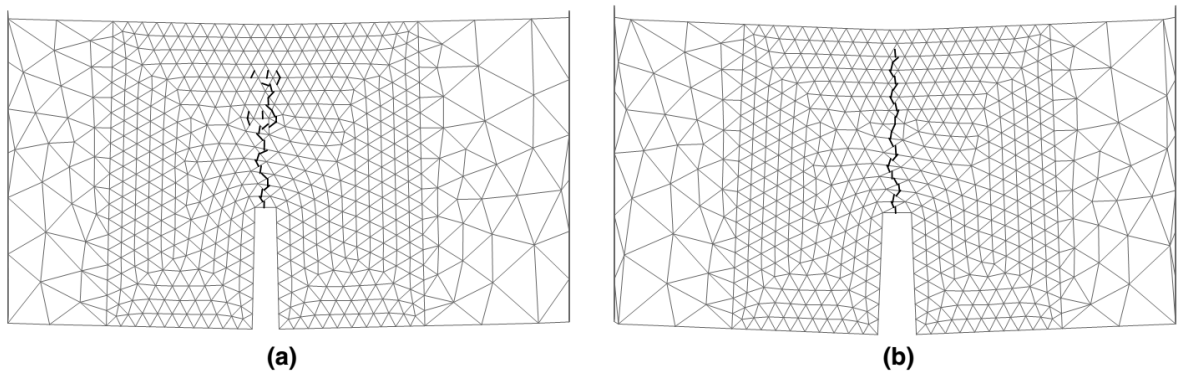

Computed crack path for the unstructured mesh: (a) without crack adaptation and (b) with crack adaptation.

Figura 41

The variables that have been used to define this material are:

- Bulk modulus;
- Shear modulus;
- Tensile strength;
- Specific fracture energy;
- Type of softening curve. In our case the shape of curve is rectangular;
- The limit of crack adaption, this parameter that has been to 5% is used for describe the last part of softening curve;
- Maximus angle of crack adaptation, like previous point;
- Tensile yield stress;
- Hard parameter;
- Type of material in our case elastic-plastic.

Simulations campaign

The modes that have been used are different for mode I and mixed mode tests. In mode I two different models have been created. The first one represents only half geometry and in the part where we have the crack propagation use cohesive material.

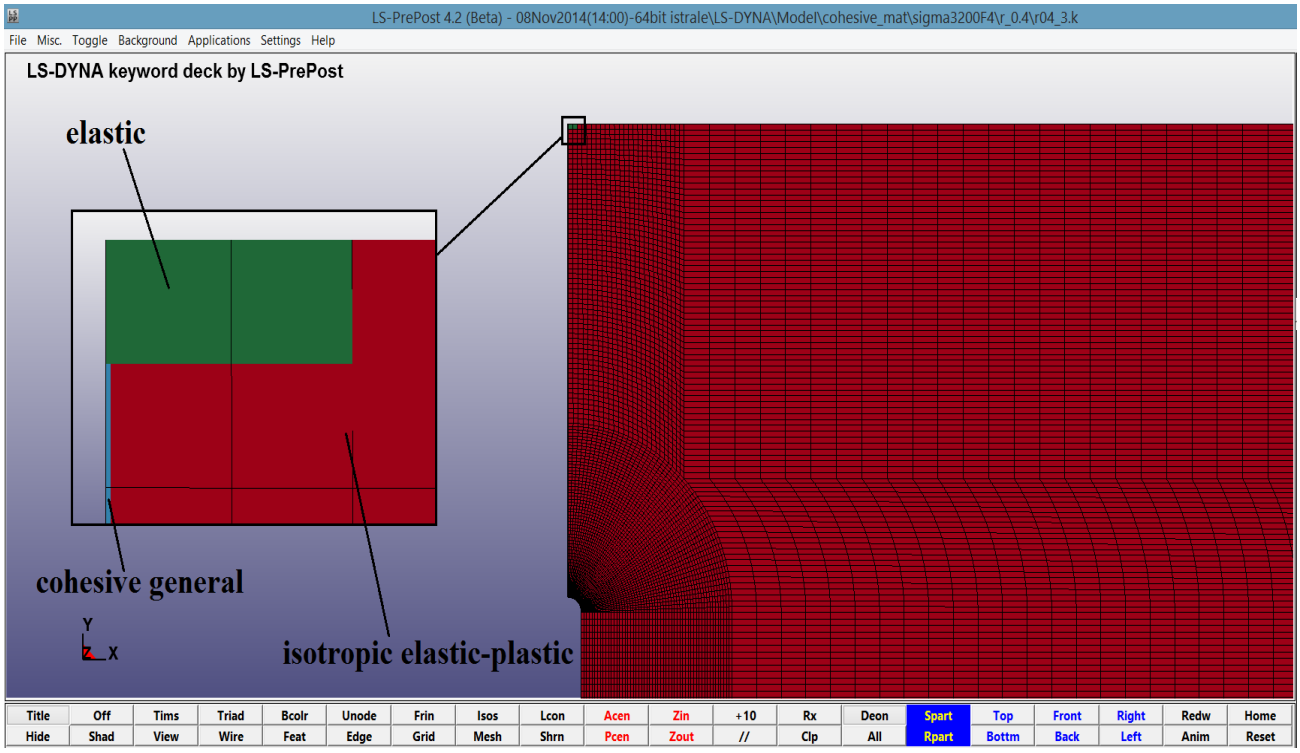

Figura 42 Simulations using cohesive general in Ls-Dyna

According to LS-Dyna principles in this model when we write the fracture toughness we must write only half of it.

The second model is based on the embedded crack approach. In this model all he geometry has been generated. This model has been used for mixed mode and also for mode I to have a second check of our results.

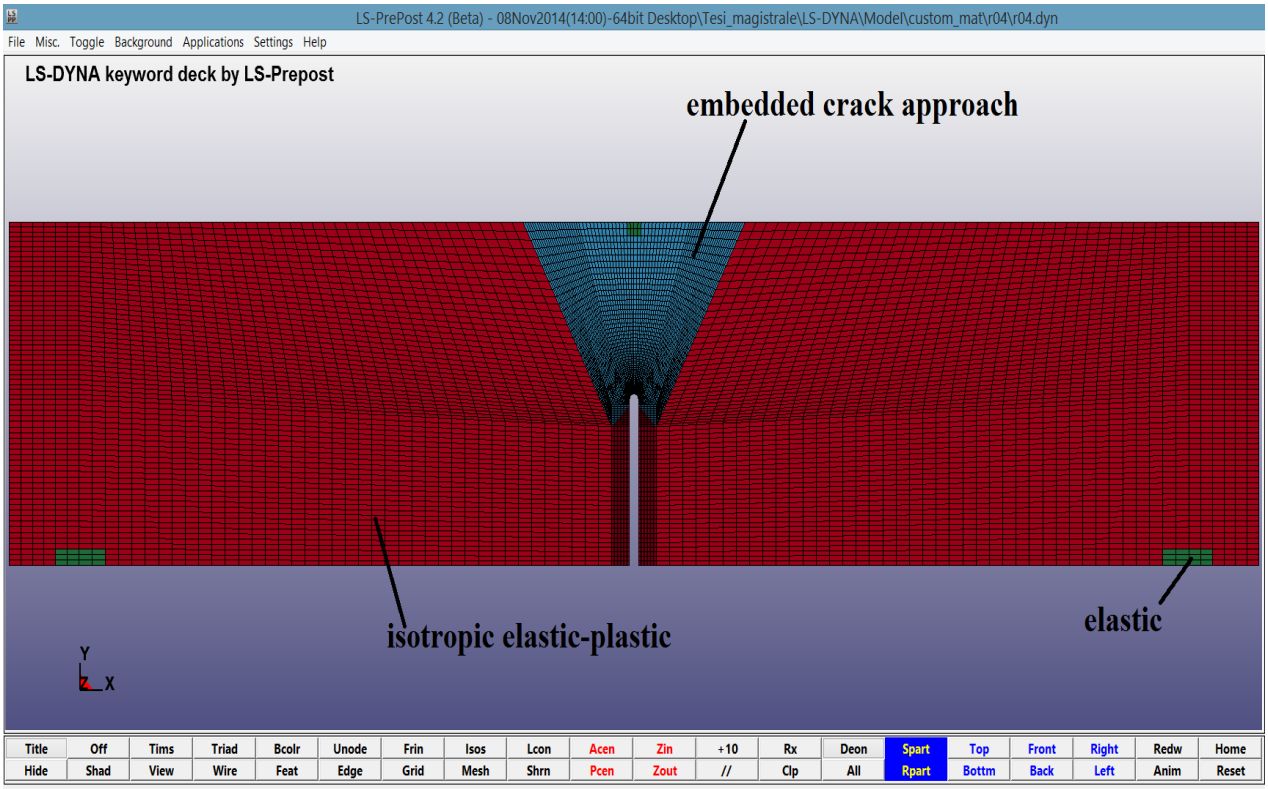

Figura 43 Simulations using embedded crack approach in Ls-Dyna

Mode I simulations using LS-DYNA

According to other experimental works in mode I simulations when we define the tensile strength we do not define the material failure tensile strength but a value that is more or less two or three time higher than tensile yield stress. In this work for define the tensile strength a number of simulations have been made, using different values of f_t for a particular radius. After that the value of f_t that make the result of simulation more similar to experimental result has been chosen. In this case like tensile strength the value of 3200 MPa has been chosen.

The schema of the tests in mode I is:

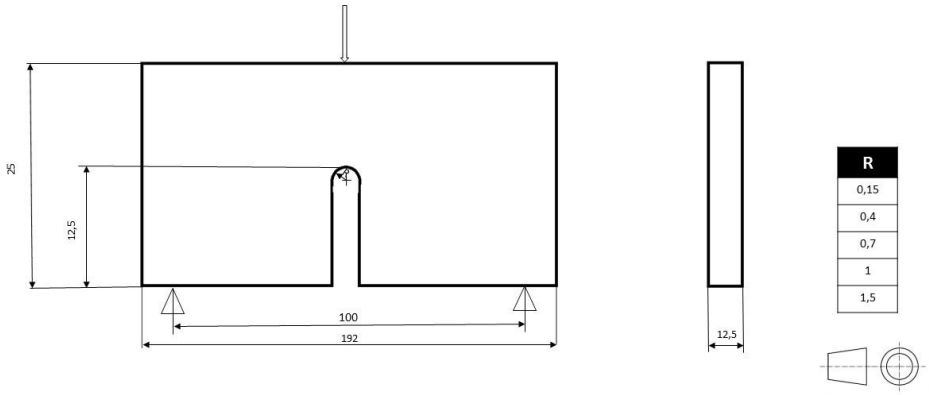

Figura 44 Mode I

The results of this first simulation campaign are:

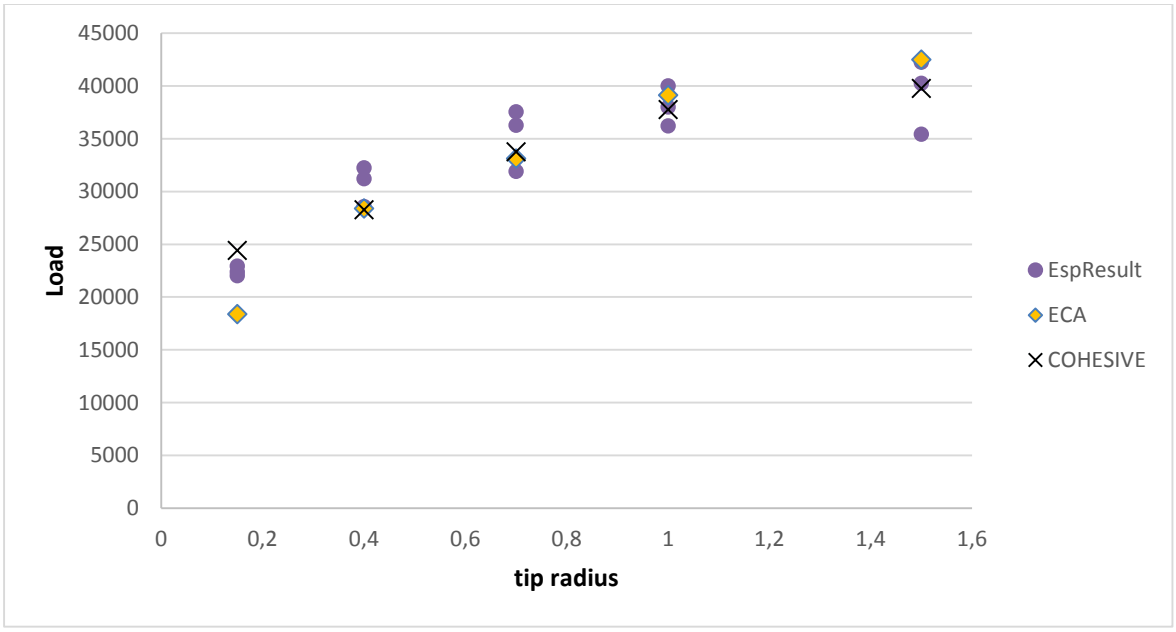

Figura 45 Mode I results using Ls-Dyna

Being ECA the results of models based on the embedded crack approach and COHESIVE are the results based on the cohesive material. EspResult are the experimental results. The exact results are:

r [mm]	cohesive	ECA
1,5	39750	42500
1	37750	39125
0,7	33750	33125
0,4	28250	28375
0,15	24425	18375

Tabella 4 Ls-Dyna Mode I results

As we can observe there is a good correspondence between the simulations and the experimental results.

Mixed Mode simulations using LS-DYNA

In these tests camping the specimens have been tested under mixed mode. These tests have been conducted with a combination or mode I and mode II. The schema of the test is:

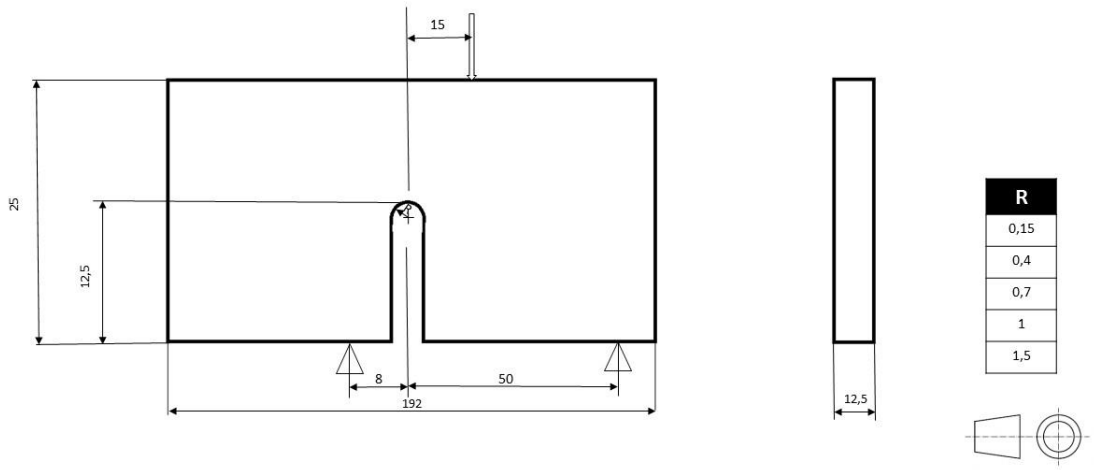

Figura 46 Mixed Mode

These tests have been conducted in LS-Dyna using only the models with the material based on embedded crack approach. There are no many results in literature about the tensile strength that has been used to describe the softening curve in this type of tests. We have tried with the same tensile strength used in mode I tests (3200MPa) and also with the failure tensile strength of material (2100MPa). In the following graph the results are plotted with the experimental results.

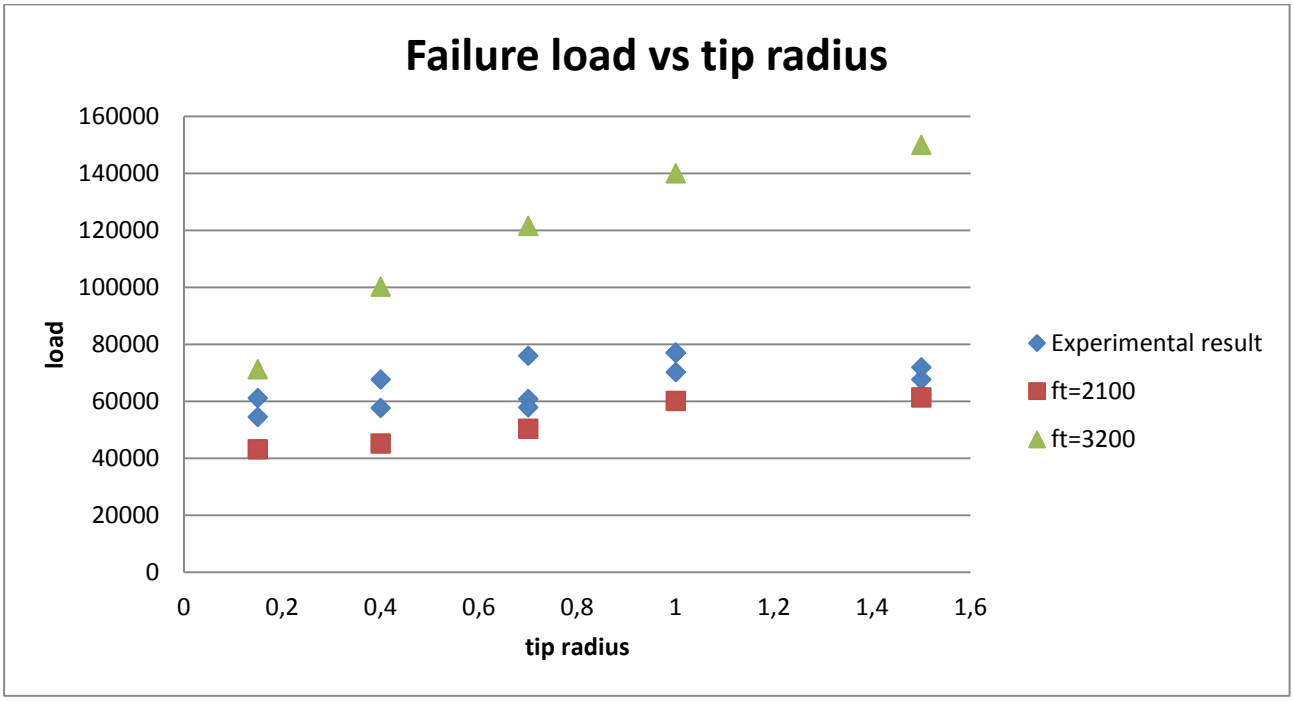

Figura 47 Mixed mode results using Ls-Dyna

The exact results can be seen in the following table:

1,5	150000	61375
1	140000	60125
0,7	121625	50375
0,4	100250	45250
0,15	71250	43125
radius	**ft=3200**	**ft=2100**

Tabella 5 Ls-Dyna Mixed mode results

These results are interesting because unlike to the results in mode I here the best value of tensile strength to approximate the experimental results is a tensile strength of 2100 MPa. We think the reason could be the influence of triaxiality. However, to obtain from simulations, not much difference between the tiraxialidad in mixed mode and mode I. A series of tests could be made, to verify that the dependence of the tensile strength with triaxiality is very high.

Strain Energy Density (SED) –

Ansys

Ansys is a finite element analysis software whose goal is the resolution, in discrete and approximate form, of general partial differential equations system. In this work the ANSYS 14.5 version has been used. The averaged strain-energy density criterion, states that brittle failure occurs when the mean value of the strain energy density over a control volume is equal to the critical energy for the un-notched material, W_C. The SED approach is based both on a precise definition of the control volume and the fact that the critical energy does not depend on the notch sharpness. The Cartesian coordinate origin is located on a certain distance r_o from the notch tip that depends both on the notch root radius (ρ) and the opening angle 2α, according to the following expression:

$$r_0 = \rho\left(\frac{\pi - 2\alpha}{2\pi - 2\alpha}\right)$$

For U-notch r_0 is simply equal to ρ/2, like in our case. If the fracture toughness K_{IC} is known the expression for critical radius R_C is, in plain strain:

$$R_C = \frac{(1+\nu)(5-8\nu)}{4\pi}\left(\frac{K_{IC}}{\sigma_u}\right)^2$$

Being: ν the Poisson's ratio and σ_u the tensile failure strength. The critical volume in U-notched specimens under mode I loading conditions is centred in relation to the notch bisector line.

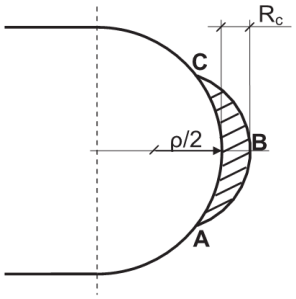

(a) Mode I

Figura 48

Under mixed mode loading the critical volume is no longer centred on the notch tip, but rather on the point where the principal stress reaches its maximum value along the edge of the notch.

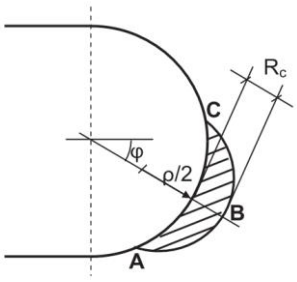

(b) Mixed mode I+II or prevalent mode II

Figura 49

The mean value of SED over the control volume for mode I can be expressed in the following form:

$$\bar{W} = H\left({}^{R_C}/_{\rho}, \nu\right)\frac{\pi\sigma_{max}^2}{4E}$$

Where σ_{max} is the maximum elastic stress at the notch tip and H is a function of R_c/ρ and ν. Function H for some values of the ratio R_c/ρ and ν is listed in some table. For mixed mode loading an equivalent expression for the averaged strain energy density has been proposed:

$$\bar{W} = H^*\left({}^{R_C}/_{\rho}, \nu\right)\frac{\pi(\sigma_{max}^*)^2}{4E}$$

Where σ_{max}^* is the maximum value of the principal stress along the notch edge and H* depends again on the normalized radius R_c/ρ the Poisson's ratio, ν, and the loading conditions. It was show that the difference between H and H* is less than 1%. According to the averaged strain-energy density criterion, failure occurs when the mean value of the SED over the control volume ($\bar{W}$) reaches a critical value (W_c).

$$W_C = \frac{\sigma_u^2}{2E}$$

In this work we have tested a quasi-brittle material. We have tried to consider the material with different material definition. The first material definition that has been

tested is linear elastic. In this assumption only the first part of Ramberg-Osgood curve has been considered.

The SED method considered only the elastic energy, therefore the Ramberg–Osgood curve has been described like a multi linear elastic curve. In this case the critical value of SED has been considered equal to the previous one. If the plastic region of material is little this assumption could be reasonable. The Equivalent Material Concept (EMC) has been used.

The Equivalent Material Concept

The Equivalent Material Concept (EMC), proposed originally by Torabi, could be able to equate a ductile material having valid fracture toughness K_{Ic} value with a virtual brittle material having the same elastic modulus and the same fracture toughness, but different tensile strength. The tensile strength of the equivalent material can be determined by considering the same value of the tensile strain energy density (SED) required for both real ductile and virtual brittle materials for the crack initiation to take place. The total SED is composed of elastic and plastic components and it can be written as:

$$(\mathrm{SED})_{\mathrm{tot}} = (\mathrm{SED})_{\mathrm{elastic}} + (\mathrm{SED})_{\mathrm{plastic}} = \sigma_u * \varepsilon_u - \int_0^{\sigma_u} \left[\frac{\sigma}{E} + \left(\frac{\sigma}{K}\right)^{1/n}\right] d\sigma$$

$$(\mathrm{SED})_{\mathrm{tot}} = \sigma_u * \varepsilon_u - \left[\left(\frac{1}{K}\right)^{1/n} \frac{\sigma^{(n+1)/n}}{(n+1)/n}\right]$$

Being K the strain-hardening coefficient, n the strain-hardening exponent, σ_u and ε_u the engineering stress and strain at maximum load.
It is possible to change the integration limits and we will obtain:

$$(\mathrm{SED})_{\mathrm{tot.}} = \frac{\sigma_Y{}^2}{2E} + \frac{K}{n+1}\left[(\varepsilon_P)^{n+1} - (\varepsilon_p^Y)^{n+1}\right]$$

If ε_P^Y is considered to be equal to 0.002 (obtained from 0.2% offset yield strength), then:

$$(\mathrm{SED})_{\mathrm{tot.}} = \frac{\sigma_Y{}^2}{2E} + \frac{K}{n+1}\left[\varepsilon_P{}^{n+1} - (0.002)^{n+1}\right]$$

If we considered a material with the same energy density but complete linear elastic:

$$(SED)_{EMC} = \frac{\sigma_f^{*2}}{2E} = (SED)_{tot}$$

And σ_f^* is the tensile strength of the equivalent material. We could easily obtain:

$$\sigma_f^* = \sqrt{\sigma_Y{}^2 + \frac{2EK}{n+1}\left[\varepsilon_{u,true}{}^{n+1} - (0.002)^{n+1}\right]}$$

In our case we did not consider the strain-hardening coefficient and the strain-hardening exponent but we had, like explained in Appendix C, the material curve.

The energy density represents the area under the material curve so using the Riemann's integral theorem we will have as follows:

$$\sigma_f^* = \sqrt{2E * (SED)_{tot}}$$

The simulation campaign

After the definition of a geometry similar to the one that has been used in Ls-Dyna we have defined:

- Element material: PLANE82 has been chosen, it is a 2-D 8-Node Structural Solid in plain strain;
- Material properties: different models have been created;
- Displacement: we had two supports that that stopped the displacement in y direction, and in one support the x displacement has been stopped for making the system isostatic;
- Load.

From a geometrical point of view, an important definition is the critical radius R_c where the SED is calculated. In our case in plain stress:

$$R_C = \frac{(1+\nu)(5-8\nu)}{4\pi}\left(\frac{K_{IC}}{\sigma_u}\right)^2 = \frac{(1+0.2)(5-8*0.2)}{4\pi}\left(\frac{40}{\sigma_u}\right)^2$$

If we consider the material σ_u that has been used is the tensile strength of material so:

$$R_C = \frac{(1+0.2)(5-8*0.2)}{4\pi}\left(\frac{40}{2100}\right)^2 = 0.000117796\, m \approx 0.118\, mm$$

In this case the critical value of Strain energy density is:

$$W_C = \frac{\sigma_u^2}{2E} = \frac{2100^2}{2*210000} = 10.5\, MPa$$

These values have been used when the material has been considered linear elastic and multi-linear elastic.

If the Equivalent Material Concept (EMC) has been used from the material curve using Riemann's integral theorem, it is possible to define the area under the curve that represents the strain energy density of our material. We then obtain:

$$(\mathrm{SED})_{\mathrm{tot}} \cong 185.3362\ \mathrm{MPa}$$

Using the formula, it is possible to define the tensile strength of the equivalent material:

$$\sigma_f^* = \sqrt{2\mathrm{E}*(\mathrm{SED})_{\mathrm{tot}}} = \sqrt{2*210000*185.3362} = 8822.766233 \approx 8823\mathrm{MPa}$$

With this value, the critical radius and the critical value of SED are:

$$R_C = \frac{(1+0.2)(5-8*0.2)}{4\pi}\left(\frac{40}{8823}\right)^2 = 0.000006673\, m \approx 0.006673\, mm$$

$$W_C = \frac{\sigma_u^2}{2E} = \frac{8823^2}{2*210000} = 185.346\, MPa$$

Results of simulation campaign

The results that we have obtained in our simulations under mode 1 are:

ρ (mm)	P_1 (N)	P_2 (N)	P_3 (N)	P linear elastic (N)	P multilinear elastic (N)	P emc (N)
1,5	40240	42264,8	35430	13079,93134	45000	49112,75927
1	38000	40000	36220	11387,47164	42500	41346,63552
0,7	31890	37560	36260	10143,22691	40000	34943,68892
0,4	32240	28560	31210	8690,006031	32500	26967,16965
0,15	22379,5	22000	22910	7729,456059	22500	17464,46506

Tabella 6 Ansys Mode I results

Being ρ the radius at notch tip. P_1, P_2 and P_3 are the experimental results, P_linear are the results obtained using a material defined linear elastic and P_multilinear considers the material multi-linear elastic. The results obtained using the equivalent material concept (emc) are illustrated in the column define P_emc.

If the results have been plotted we obtained the follow chart:

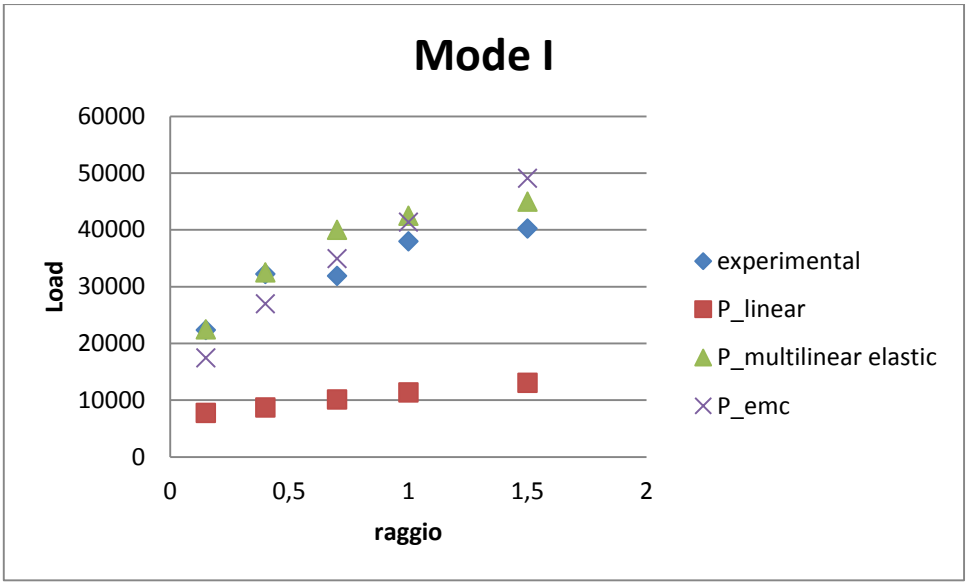

Figura 50 Mode I results using Ansys

If we had considered the material linear elastic the results are smaller than experimental one. It is possible to see that the results obtained considering the equivalent material concept and multi-linear elastic definition are similar. We have tried to make a path along the bisector in the control volume and the first principal stress has been plotted:

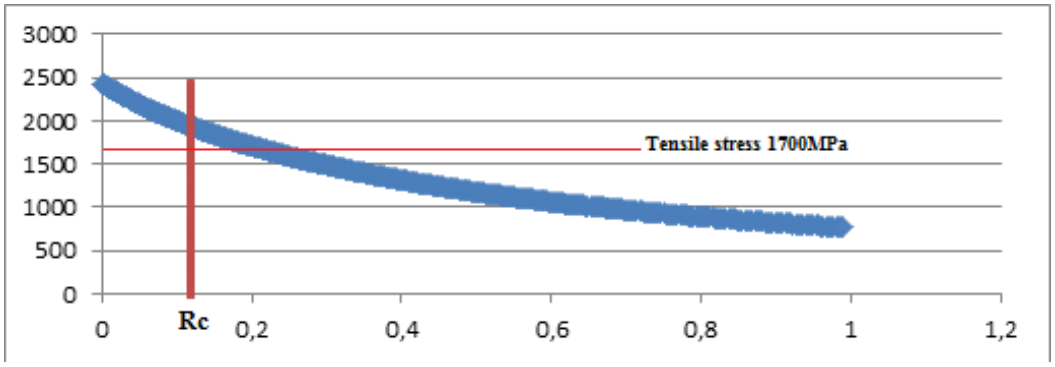

Figura 51 Path

It possible to see that in all the control volume the stress is bigger than in the tensile stress. Therefore, in the control volume the material works in plastic region.

Working in plastic region the linear elastic definition cannot be used to predict the failure load of material. The results for the material works in mixed mode are:

ρ (mm)	P_1 (N)	P_2 (N)	P_3 (N)	P linear elastic (N)	P multilinear elastic (N)	P emc (N)
1,5	67651,37	62433,47	71946,72	46032,24949	150000	172623,8681
1	77067,6	77045	70226,7	40763,51691	147500	147341,7916
0,7	60817	76037	57894,3	36849,40023	137500	126939,0084
0,4	67703,55	57651,06		31029,74606	98750	99540,33453
0,15	61210	54575,81		24470,63406	71250	64591,99319

Tabella 7 Ansys mixed mode reults

These results that have been plotted on the chart, represent the failure load versus the tip radius, and the results are:

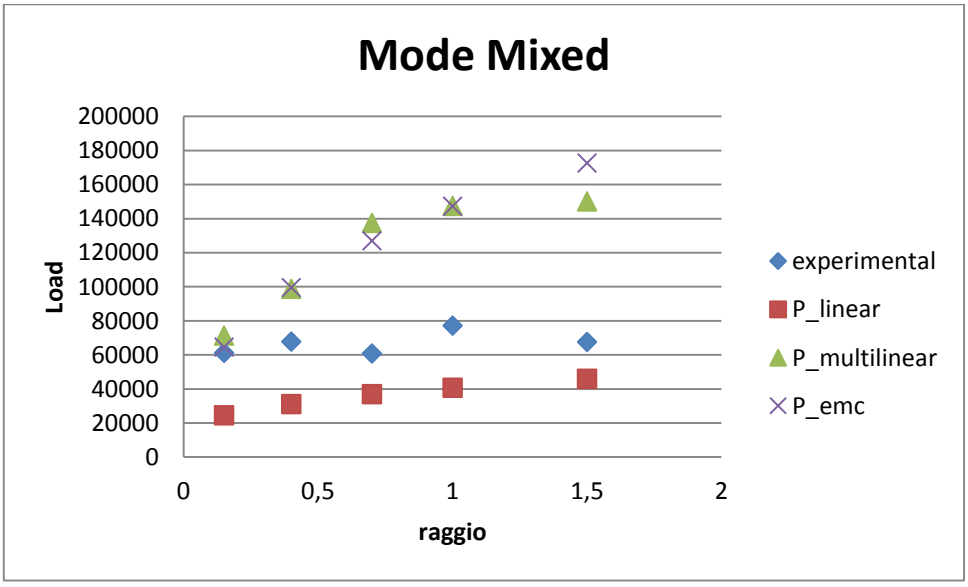

Figura 52 Mode mixed results using Ansys

In this case we can see that the results that considered the material multi-linear elastic are too high compared to the results that used the equivalent material concept.
The results considering the material linear elastic are better but not quite near to the experimental ones.

Conclusion

If all the result obtained are put together:

Mode	ρ (mm)	P_1 (N)	P_2 (N)	P_3 (N)	Pavarage (N)	P linear elastic (N)	P multilinear elastic (N)	P emc (N)	P_cohesive (N)	P_eca (N)
I	1,5	40240	42264,8	35430	40240	13079,93134	45000	49112,75927	39750	42500
I	1	38000	40000	36220	38000	11387,47164	42500	41346,63552	37750	39125
I	0,7	31890	37560	36260	36260	10143,22691	40000	34943,68892	33750	33125
I	0,4	32240	28560	31210	31210	8690,006031	32500	26967,16965	28250	28375
I	0,15	22379,5	22000	22910	22379,5	7729,456059	22500	17464,46506	24425	18375
mixed	1,5	67651,37	62433,47	71946,72	67651,37	46032,24949	150000	172623,8681		150000
mixed	1	77067,6	77045	70226,7	77045	40763,51691	147500	147341,7916		140000
mixed	0,7	60817	76037	57894,3	60817	36849,40023	137500	126939,0084		121625
mixed	0,4	67703,55	57651,06		62677,31	31029,74606	98750	99540,33453		100250
mixed	0,15	61210	54575,81		57892,9	24470,63406	71250	64591,99319		71250

Tabella 8 Total results

Being:

Name	definition of failure load	support
Pavarage	median of experimental results	
P linear	considering the material linear elastic	Ansys
P multilinear	considering the material multi-linear elastic	Ansys
P emc	equivalent material concept	Ansys
P_cohesive	using cohesive general material type	Ls-Dyna
P_eca	using embedded crack approac	Ls-Dyna

Tabella 9 Legenda

An interesting thing is to plot all the results for mode I and for mixed mode:

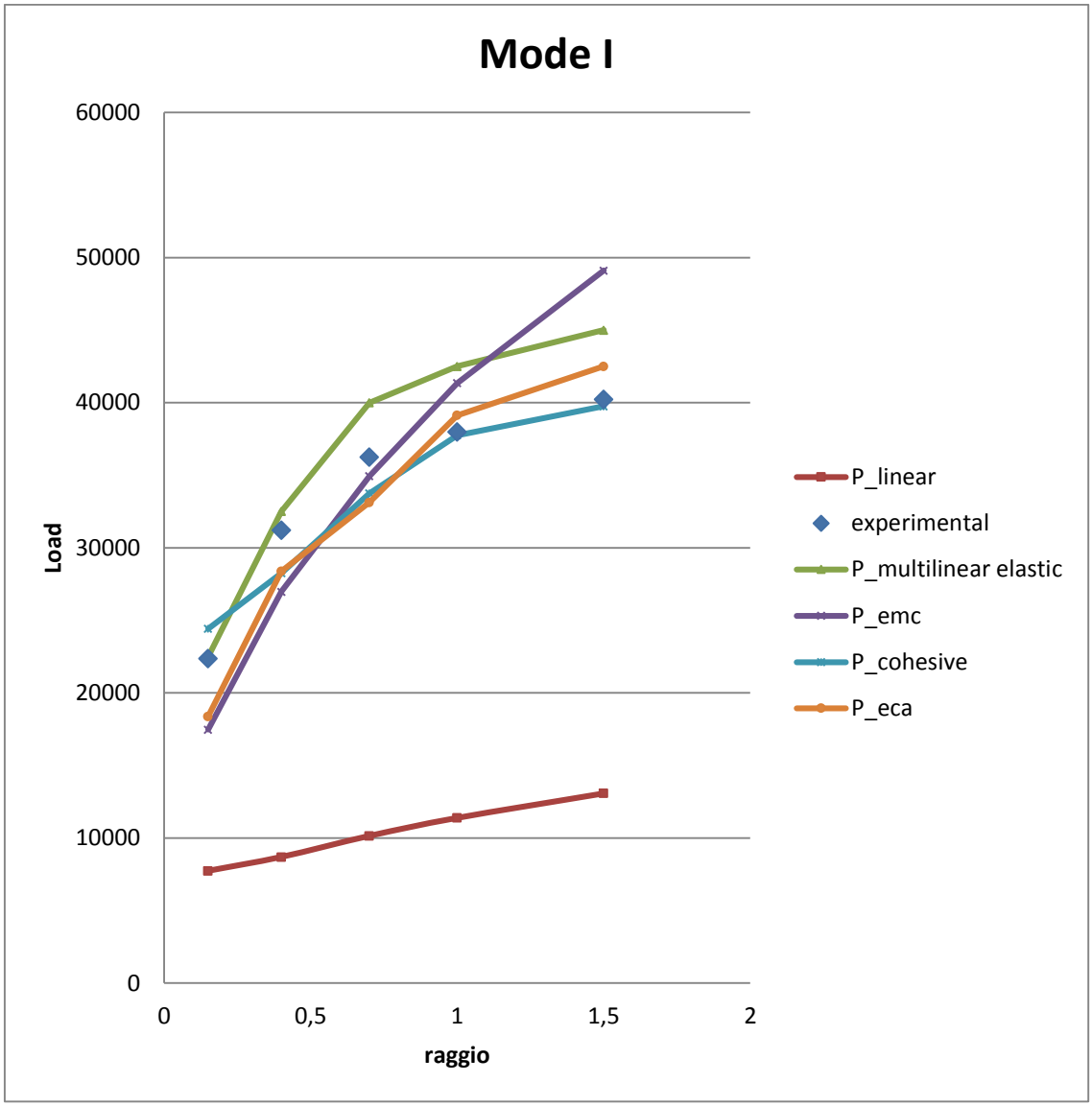

Figura 53Total mode I results

The methods that have been used, except for linear elastic definition, generate a good characterization of failure load. Although the results are good, another aspect must be considerate: the time for realising the simulations. The methods that have used Ls-Dyna were slow and every simulation took hours. The methods in Ansys are faster but using a material defined as multi-linear elastic needs some minute to converge to a solution. The method with an excellent correlation with experimental results and speed is the method based on equivalent material concept (emc).

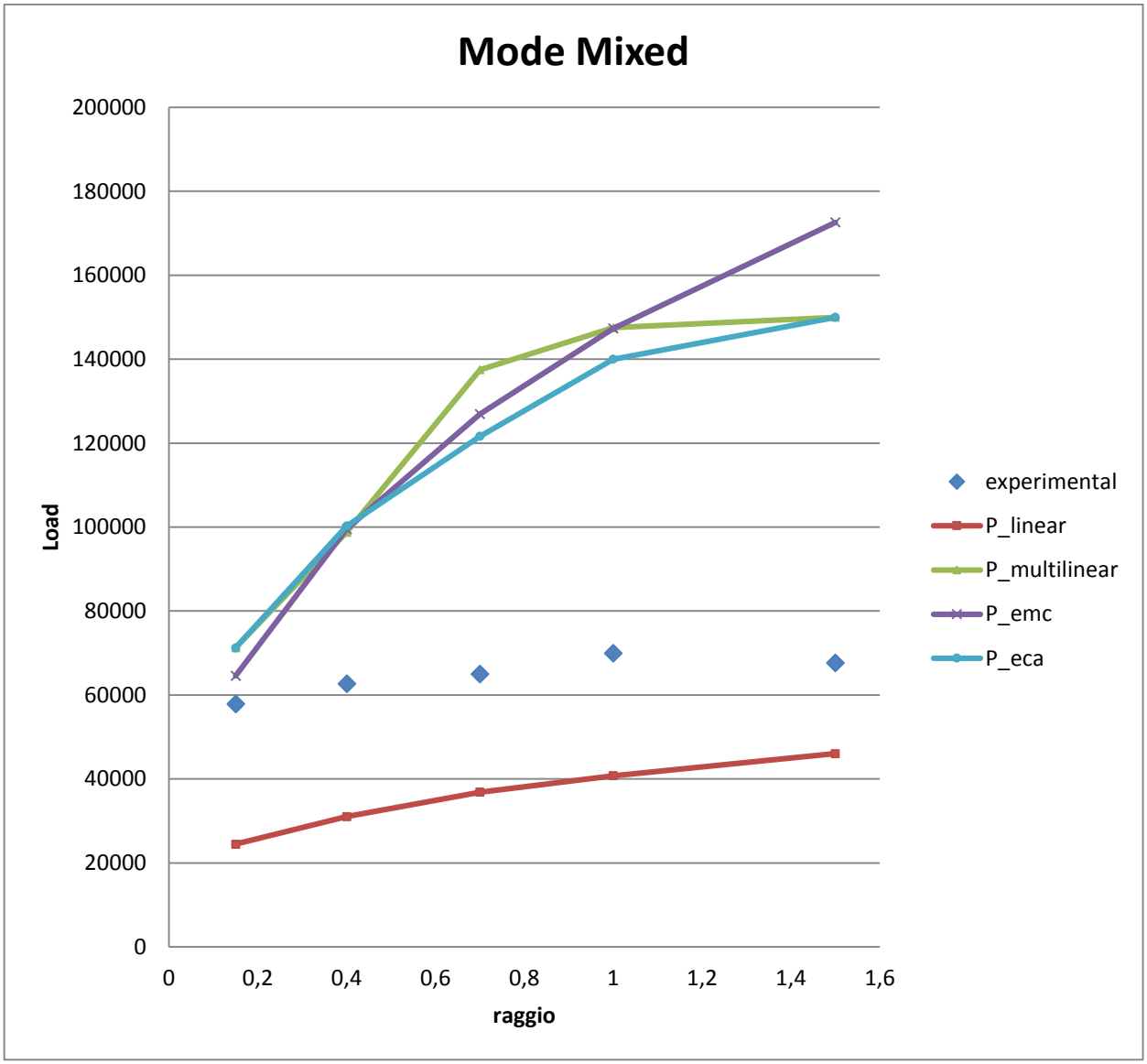

Figura 54 Total Mixed Mode results

For mixed mode simulation the results of simulations are not good.

The material that was studied, presents a behaviour that deviates from the linear elastic one and shows a large part of the energy, which occurs in the plastic range, has dissipated. In case of mixed mode the experimental results are different from simulation campaigns.

In our consideration only the influence of Mode I has been considered. In mixed mode cases the maximum load is not in the top of notch but approximately at 53°.

The crack in the experimental campaign starts approximately where start the tip radius. From these results we could deduced that the influence of triaxiality is important. If we considered also the effects of mode II the value of critical radius must change. For a tip radius of 1 mm the average failure load is 77045 N. We have tried to change the value of critical radius in these conditions and we have seen the behaviour of SED. The results are:

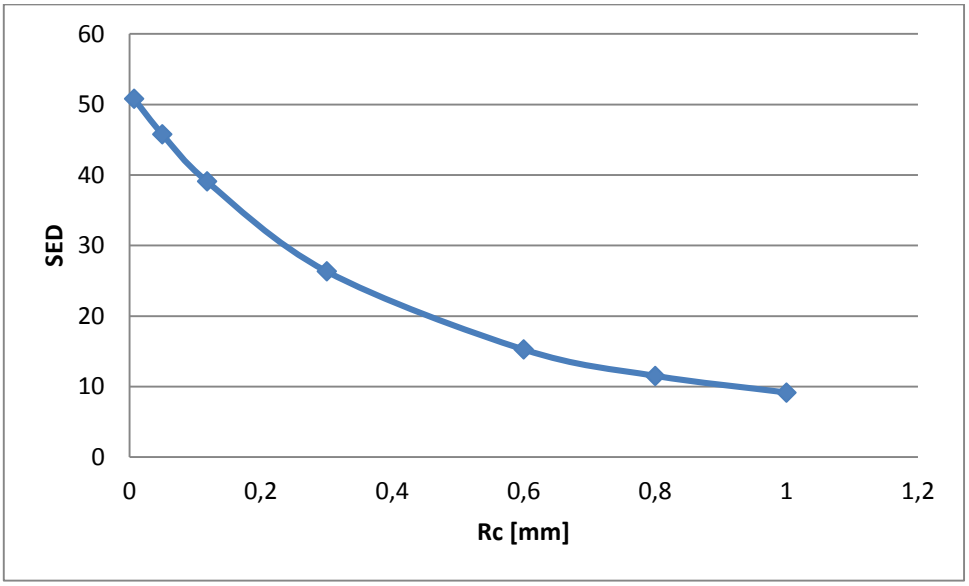

Figura 55

If the critical value of SED is equal to the one that has been previously considered, a bigger critical radius must been chosen. We see that a critical radius must be around 0.85 mm.

Future development

One of the future developments that have common interests for both the models used is the extension of the experimental campaign, changing the geometry of the notch and the kind of loading. It is interesting to test other geometries to check if the methods, that have been used, are able to provide good approximations of failure load and the behaviour of the material with different geometries.

For the material characterization an experimental campaign is scheduled to check the sensibility of material to triaxiality. This is as to understand why in mixed mode our simulations generated so bad results.

Regarding the cohesive model, the next step is the introduction of the effect of the variation of behaviour in the model, varying the triaxiality, inside the subroutine which describes Hencky's model for the cohesive crack model.

Another possible step, is trying to obtain the right parameter to describe the softening curve. The fracture energy is complicated to derive, because a cylindrical specimen with a circumferential crack will be created. In this work the softening curve chosen was not verify experimentally. An experimental verification of softening curve could be doing.

Appendix A

Special requirements for the testing of bend specimens

The procedure has been followed so the valor of K is the most accurate possible. The procedure that has been used is the E399-90. It is desirable to fatigue crack the bend specimen in the same fixtures in which it will be tested so that the K calibration is accurately known. However, bend specimens are sometimes cracked in cantilever bending because this method permits ease of reversed loading. If the K calibration for three-point bending is used in cantilever bending, the bending moments for a given K value will be underestimated. While fatigue cracking in cantilever bending can yield satisfactory results, it should be emphasized that the crack tip stress field can be distorted and the fatigue crack orientation changed by excessive clamping forces.
Apparatus

- Bend Test Fixture: This fixture is designed to minimize frictional effects by allowing the support rollers to rotate and move apart slightly as the specimen is loaded, thus permitting rolling contact. Thus, the support rollers are allowed limited motion along plane surfaces parallel to the notched side of the specimen, but are initially positively positioned against stops that set the span length and are held in place by low-tension springs (such as rubber bands).

- Displacement Gage: For the bend specimen the displacements will be essentially independent of the gage length up to a gage length of W/2.

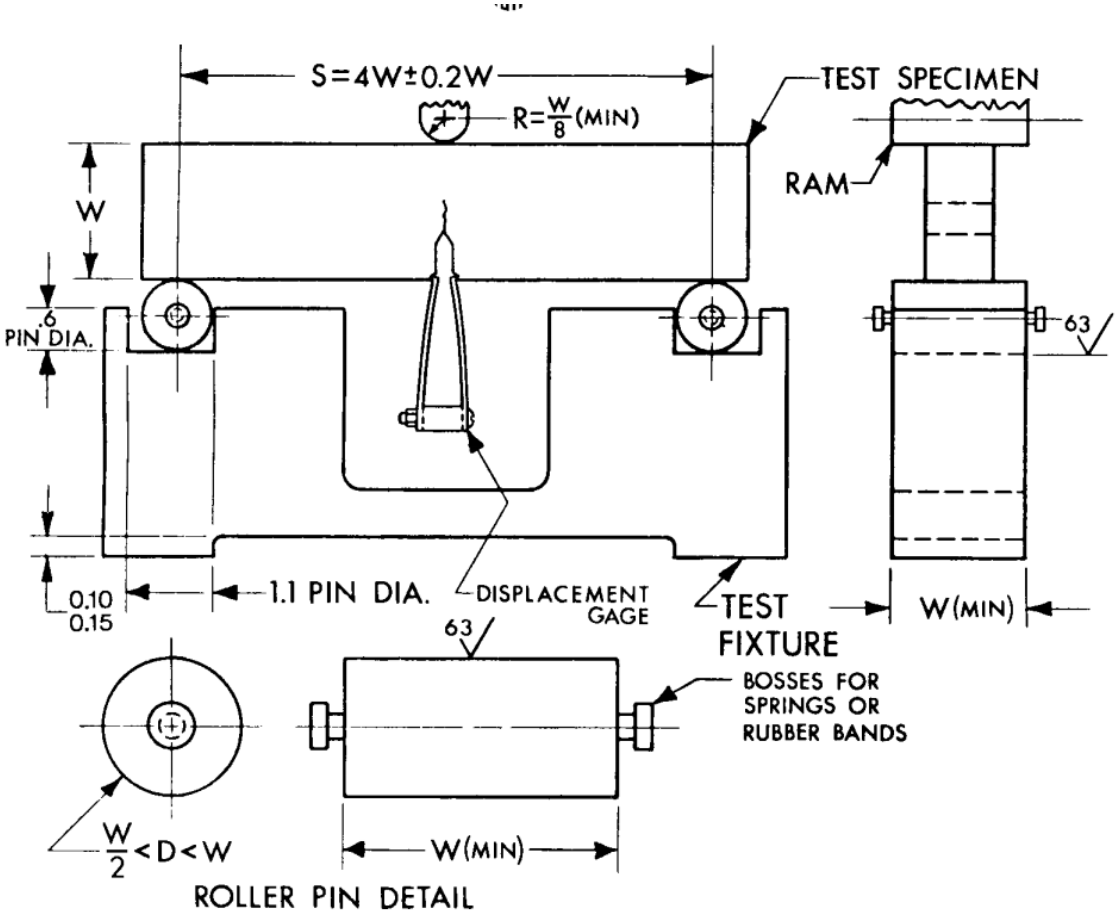

Appendix A figure 1

Procedure

- Measurement: for a bend specimen measure the width (depth), W, and the crack length, a, from the notched side of the specimen to the opposite side and to the crack front, respectively.
- Set up the test fixture so that the line of action of the applied load shall pass midway between the support roll centers within 1 % of the distance between these centers (for example, within 0.04 in. (1.0 mm) for a 4-in. (100-mm) span). Measure the span to within 0.5 % of nominal length. Locate the specimen with the crack tip midway between the rolls to within 1 % of the span, and square to the roll axes within 2°. Seat the displacement gage on the knife edges to maintain registry between knife edges and gage grooves. In the case of attachable knife edges, seat the gage before the knife edge positioning screws are tightened.

- Load the specimen at a rate such that the rate of increase of stress intensity is within the range 30 to 150 ksi·in.1/2/min (0.55 to 2.75 MPa·m0.5/s), corresponding to a loading rate for the standard (B 5 0.5 W) 1-in. (25.4-mm) thick specimen between 4000 and 20 000 lbf/min (0.30 to 1.5 kN/s)

Calculation:

For the bend specimen calculate K_Q in units of ksi·in.1/2 (MPa·m0.5) as follows

$$K_Q = \left(\frac{P_{Q*} * S}{B * W^{3/2}}\right) * f(a/W)$$

Where:

$$f(a/W) = \frac{3\left(\frac{a}{W}\right)^{\frac{1}{2}}\left[1.99 - \left(\frac{a}{W}\right)\left(1 - \frac{a}{W}\right)\left(2.15 - 3.93\frac{a}{W} + 2.97\frac{a^2}{W^2}\right)\right]}{2\left(1 - 2\frac{a}{W}\right)\left(1 - \frac{a}{W}\right)^{\frac{3}{2}}}$$

being:

P_Q = load as determined, klbf (kN),

B = specimen thickness in. cm

S = span as determined in. cm

W = specimen depth (width), in cm

a = crack length, in. cm

To facilitate calculation of KQ, values of f(a/W) are tabulated in the following table for specific values of a/W:

Bend Specimens			
a/W	*f(a/W)*	*a/W*	*f(a/W)*
0.450	2.29	0.500	2.66
0.455	2.32	0.505	2.70
0.460	2.35	0.510	2.75
0.465	2.39	0.515	2.79
0.470	2.43	0.520	2.84
0.475	2.46	0.525	2.89
0.480	2.50	0.530	2.94
0.485	2.54	0.535	2.99
0.490	2.58	0.540	3.04
0.495	2.62	0.545	3.09
		0.550	3.14

Appendix A Tabella 1

For pre-crack the specimens we have supposed a value of f(a/W)=2.66, S=10cm, W=2.5cm and B=1.25cm with a P=1KN we obtain a K_Q=1.314MPa $m^{0.5}$. In our hypothesis it has been supposed a fracture toughness more or less of 35 MPa $m^{0.5}$, and using a safety factor of 80% we obtained a P_Q=5.20156KN and this was our limit value. The machine that has been used is the INSTRON machine, model8803 it is a hydraulic machine. We imposed a load limit of ±5KN. The pre-crack part was made with a sinusoidal load cycling. The pre-crack part was divided in three parts. In the first and in final one a mean stress of 1.6KN, an amplitude of 1.4KN and a frequency of 10Hz has been imposed. In the second part, has used a mean stress of 2KN, an amplitude of 1.6KN and a frequency of 15Hz. To control the crack a camera Pro Res capture Pro 2.6 was employed, with the use of program Vic Snap LSE298-03 for check the crack propagation. After more or less 20000 cycle s, the cycling part has been stopped. The control machine has been imposed in linear and a TPB (three point bending) test has been made. The initial idea was of testing 5 specimens, but one broke due to an excessive load in the first test and another one broke during the cycling part. After the test the specimen has been photographed and using the

program ImageJ the real crack length has been founded. Using the preview formulas the real fracture toughness has been revealed.

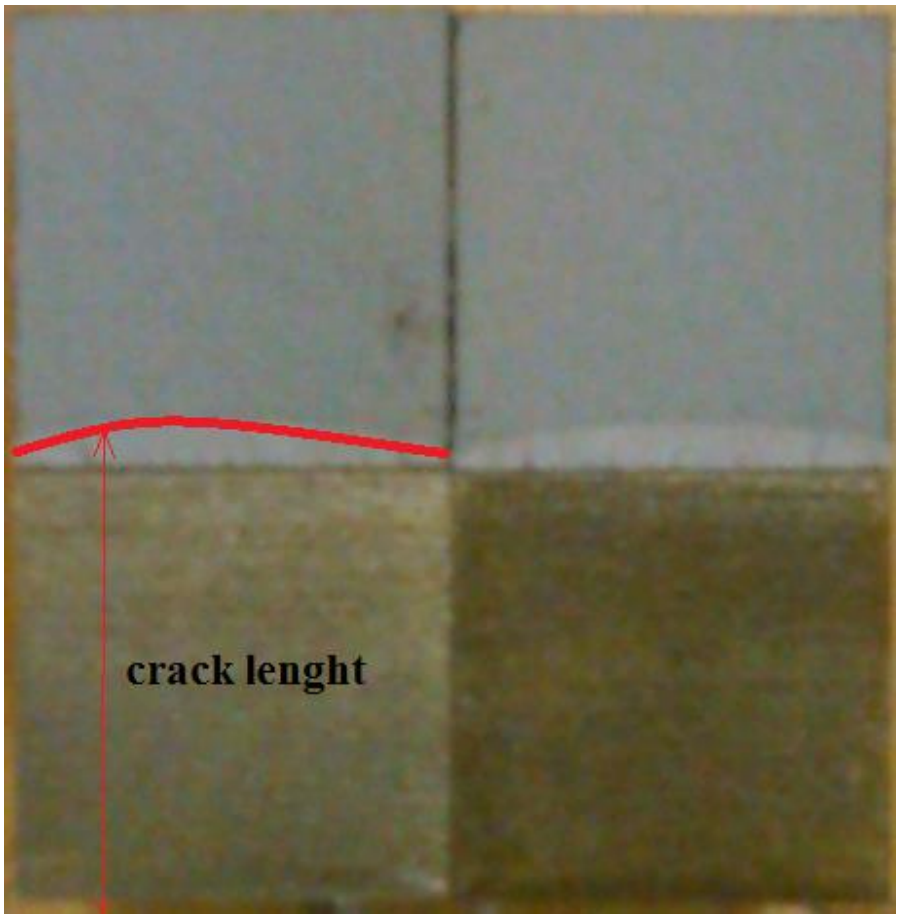

Appendix A figure 2

The not perfect linearity of crack length could be determined by a displacement of the specimen from its position. The following table shows the result of the specimens used where:

P_Q = failure load determined in the test, klbf (kN),
B = real specimen thickness, in. (cm),
S = span as determined in. (cm),
W = real specimen depth (width), in (cm),
a = medium value of crack length calculate from picture, in. (cm),

K_Q = determined with the previous formula (MPa $m^{0.5}$)

Specimes	PQ	S	B	W	a/W	f(a/W)	KQ
XVI	6.736	10	1.26	2.54	0.537267	3.09	40.80745
XVII	7.229	10	1.26	2.53	0.515078	2.84	40.48976
XX	6.844	10	1.265	2.54	0.533305	3.04	40.62959

Appendix A Tabella 2

The value used in the simulation was 40 MPa $m^{0.5}$ and it is a good approximation of real value.

Appendix B

Verify of the radiuses of curvature of the notch

The figure shows the geometry of the notched specimens. The only difference between the geometries is the radius of curvature of the notch r

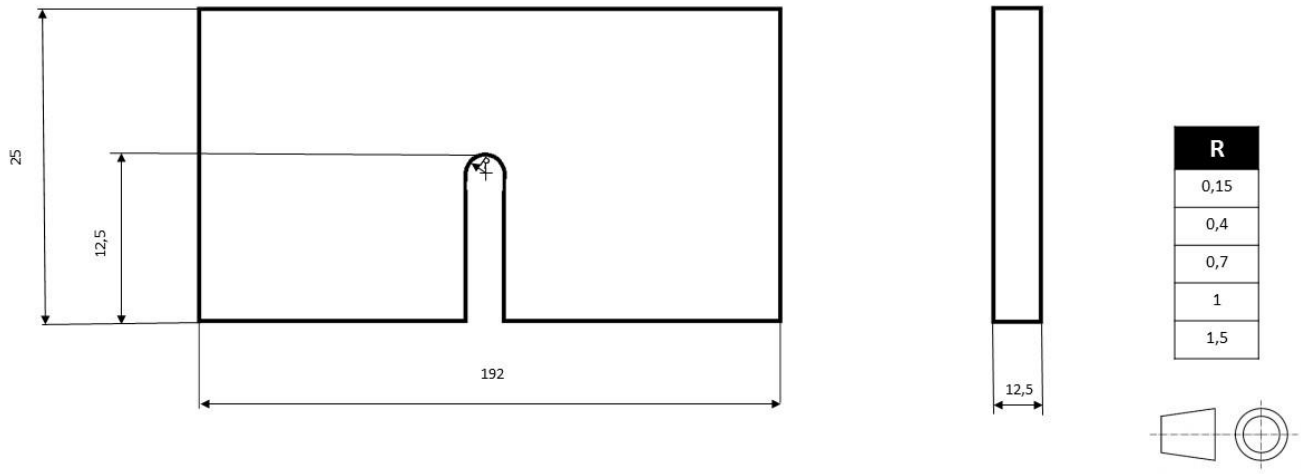

Appendix B figure 1

Once prepared the specimens, before the testing, it is necessary to check if the notch radii are approximately the same of the theoretical values. We check because, more is the affecting of small dimensional changes due to processing that can lead to significant differences between the theoretical value and the actually measured one. In addition to this possible error, the shape of each notch radius should also be checked because small defects that are unperceivable with the naked eye could act as stress concentrators that could lead to unexpected results.

In order to verify the radii of curvature of the notch, a deep analysis of the actual geometry of the same has been made. Such verification was started with a profile projector, but its zoom capability made it impossible to measure the radii of curvature smaller than a millimetre.

Appendix B figure 2

To get a more accurate control it was decided to use a transmission optical microscope, which coupled with a calibrated grid and an image analysis program (ImageJ) that allows to interpolate various points taken from the radius, permitting to find the circumference which best interpolates the various points. The microscope is a

Nikon Metaphot and the camera that has been used for capturing the image is a ProgRes C5 made by Jenoptik German.

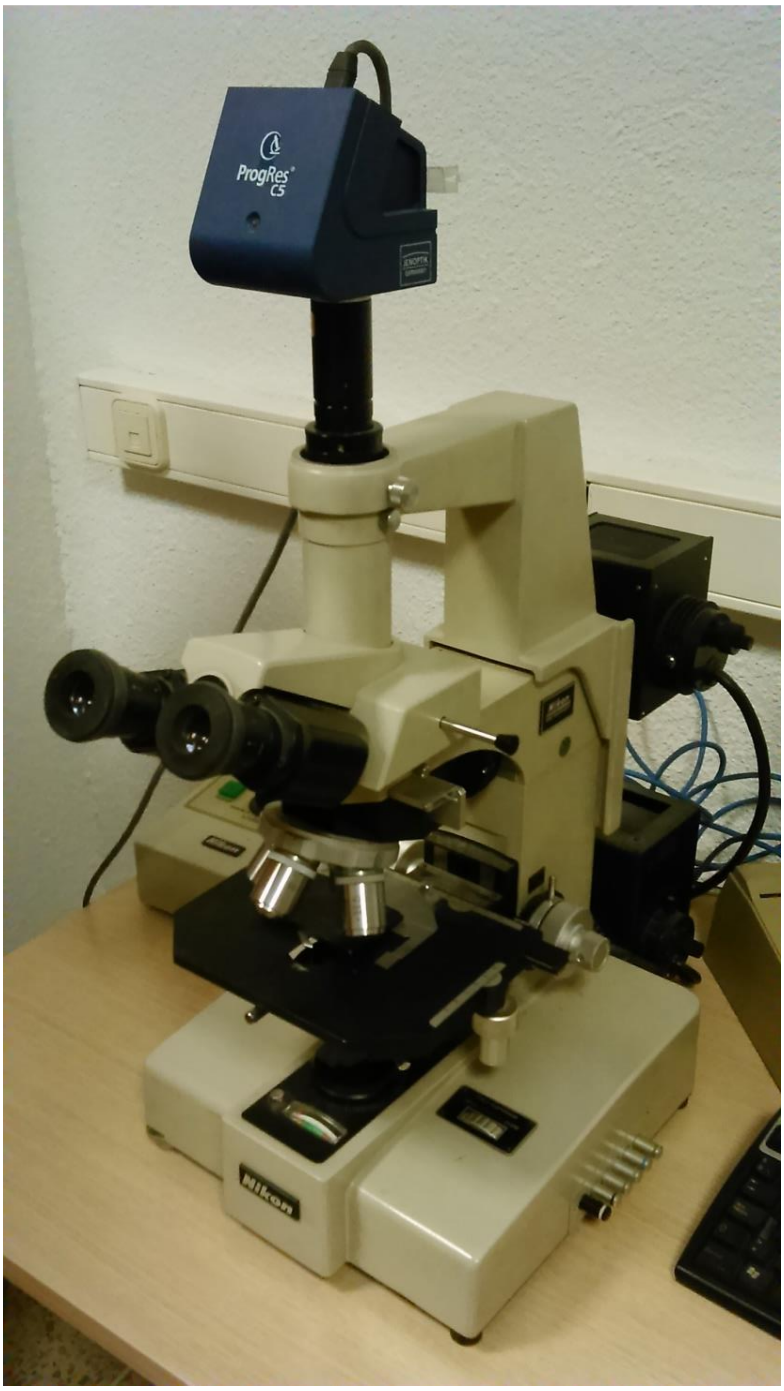

Appendix B figure 3 microscope

The program, ImageJ, uses the Feret’s diameter. Feret's diameter is a measurement of an object size along a specified direction. In general, it can be defined as the distance between the two parallel planes restricting the object perpendicular to that direction.

It is therefore also called the caliper diameter, referring to the measurement of the object size with a caliper. This measure is used in the analysis of particle sizes, for example in microscopy, where it is applied to projections of a three-dimensional (3D) object on a 2D plane. In such cases, the Feret diameter is defined as the distance between two parallel tangential lines rather than planes.

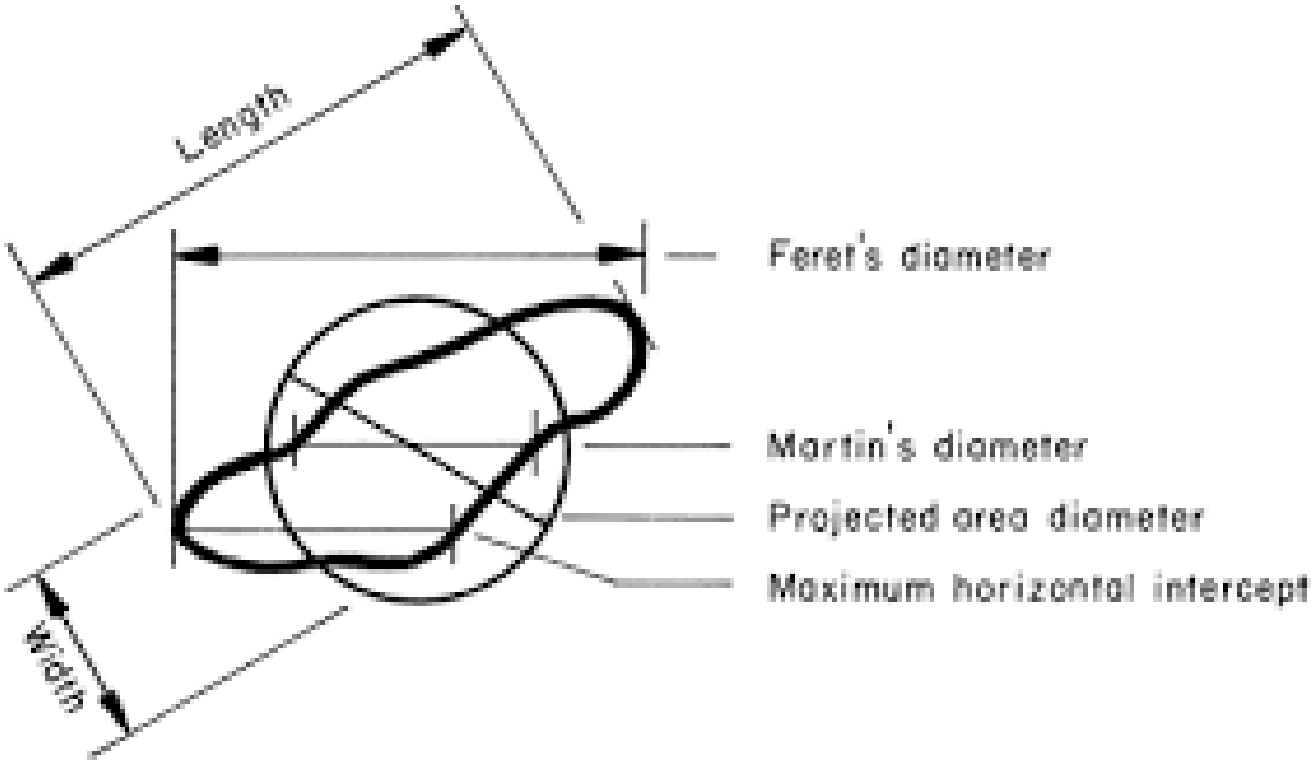

Appendix B figure 4 Feret's diameter

Given that the program processes digitalized images, the size of the circumference that is provided is in pixels. It was therefore necessary to use a measuring grid, also photographed by the microscope, for every enlargement available, so as to be focused as the specimens, through which it is possible to obtain a connection between the number of pixels and the number of millimeters in the taken images. In the following figure it is possible to see the grid that has been used for the enlargement 10.

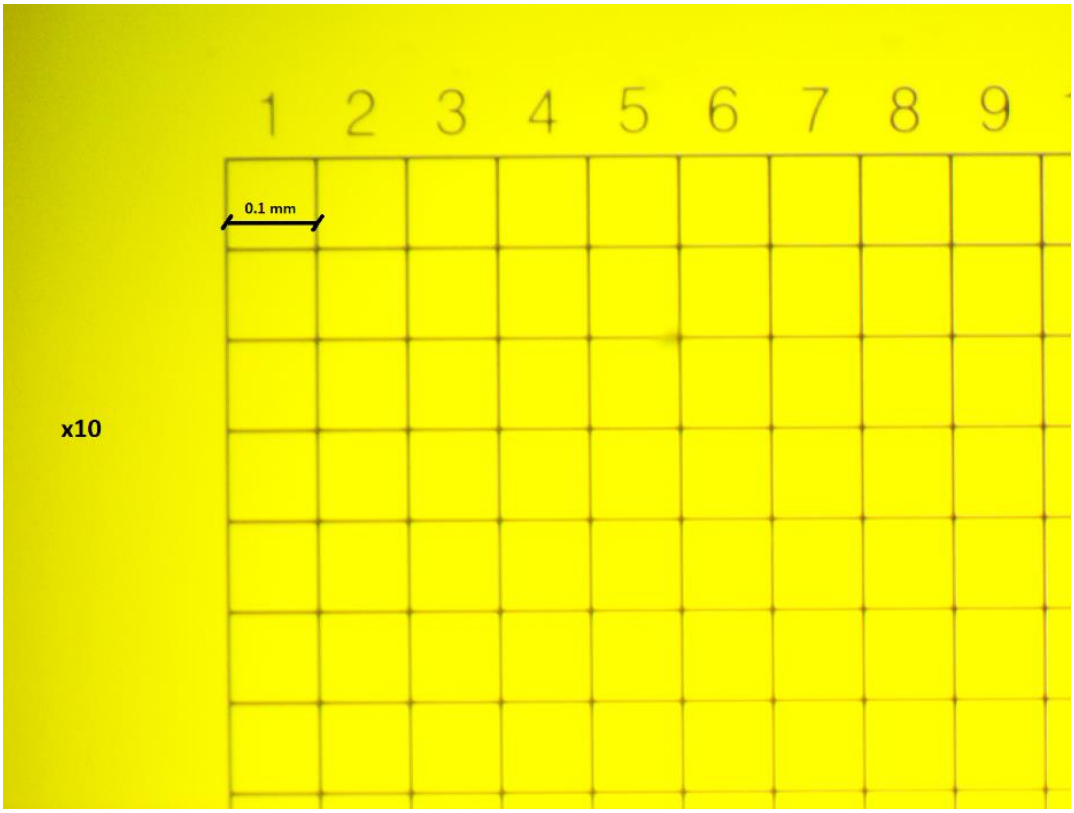

Appendix B figure 5 Calibration

Example of process of the curvature radii measurement:

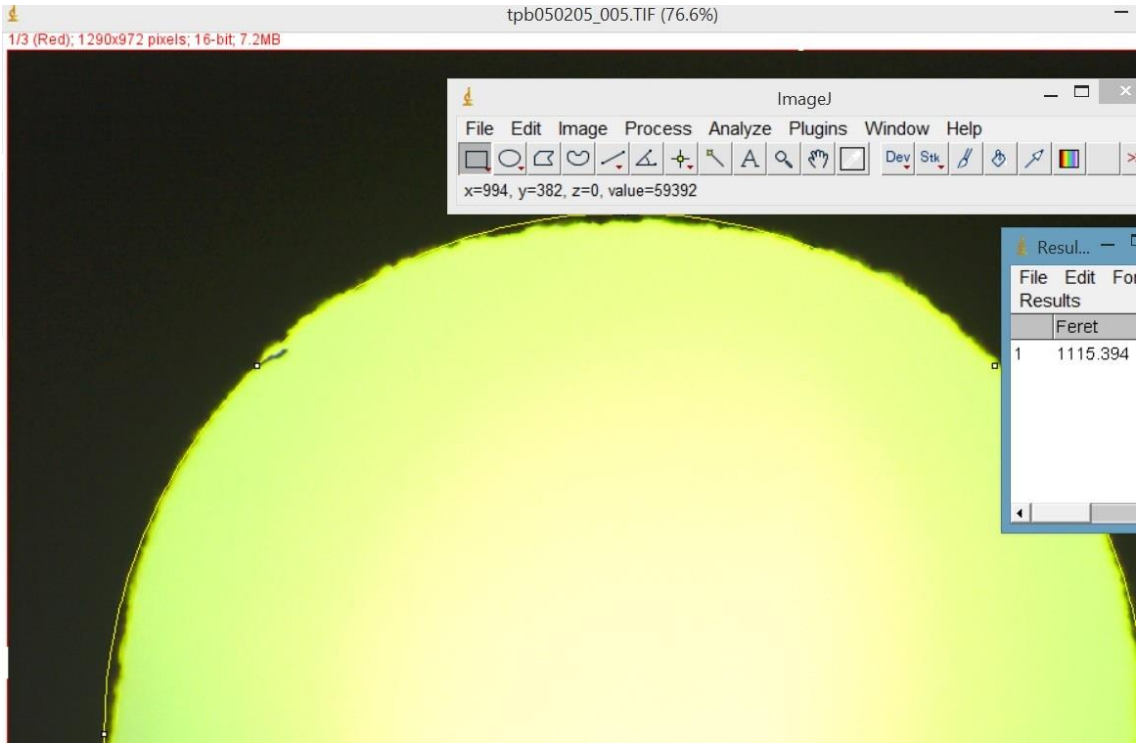

Appendix B figure 6

When the correlation between pixel and mm has been founded it is easy to get the effective tip radius for every specimen.

Below there is a table that summarizes the results of this verification for the specimens that have been used in the test under mode I and for the verification of fracture toughness:

specimen name		Enlargement	nominal	radius [mm]
tpb050205_001	I	5	1,5	1,488
tpb050205_002	II	5	1,5	1,493
tpb050205_003	III	5	1,5	1,497
tpb050205_004	IV	20	0,15	0,152
tpb050205_005	V	5	1	1,016
tpb050205_006	VI	5	1	1,027
tpb050205_007	VII	5	1	1,02
tpb050205_008	VIII	10	0,7	0,686
tpb050205_009	IX	10	0,7	0,698
tpb050205_010	X	10	0,7	0,711
tpb050205_011	XI	20	0,15	0,157
tpb050205_012	XII	20	0,15	0,157
tpb050205_013	XIII	10	0,4	0,41
tpb050205_014	XIV	10	0,4	0,402
tpb050205_015	XV	10	0,4	0,424
tpb050205_016	XVI	20	0,15	0,158
tpb050205_017	XVII	20	0,15	0,156
tpb050205_018	XVIII	20	0,15	0,159
tpb050205_019	XIX	20	0,15	0,158
tpb050205_020	XX	20	0,15	0,156
tpb050302_001	XXI	5	1,5	1,498
tpb050302_002	XXII	5	1,5	1,492

Appendix B tabella results 1

The specimens XXI and XXII have been added because two tests with radius of 1.5mm broke for an anomalous failure load. As it can be seen in the previous table that summarized the measures of the radius of curvature of the notch, the real radius measures for the 0,15 mm specimens was at least 50% greater than the theoretic one while, in the other geometry the measures were equal to the theoretic ones.

The same procedure has been followed to verify also the specimens that have been used in the test under mixed mode. The result is summarized in the following table:

specimen name		enlargement	nominal	radius [mm]
tpb050302_003	XXIII	5	1	1,007
tpb050302_004	XXIV	5	1	0,995
tpb050302_005	XXV	5	1	0,998
tpb050302_006	XXVI	5	1	0,99
tpb050302_007	XXVII	5	1	0,998
tpb050302_008	XXVIII	5	1	0,992
tpb050302_009	XXIX	5	0.7	0,702
tpb050302_010	XXX	5	0,7	0,708
tpb050302_011	XXXI	5	0,7	0,703
tpb050302_012	XXXII	10	0,4	NO
tpb050302_013	XXXIII	10	0,4	0,406
tpb050302_014	XXXIV	10	0,4	0,405
tpb050302_015	XXXV	20	0,15	0,164
tpb050302_016	XXXVI	20	0,15	0,165
tpb050302_017	XXXVII	5	1,5	1,504
tpb050302_018	XXXVIII	5	1,5	1,499
tpb050302_019	XXXIX	5	1,5	1,495
tpb050302_020	XL	5	1,5	1,49

Appendix B tabella results 2

Also for this specimens it is possible to see in the previous table that summarized the measures of the radius of curvature of the notch, the real radius measures for the 0,15 mm specimens are greater than the theoretic one while, in the other geometry the measures were equal to the theoretic ones.

For both the series of specimens it is possible to say that there is a good correlation between the real and the nominal radii.

Appendix C

Determination of material proprieties

The material properties have been determined using a ‘dog bone’ specimen. In this experimental campaign four specimens have been used. The specimens used can be seen in the following figure:

Appendix C figure 1 Specimen

To tests, an INSTRON machine, model 8501 a hydraulic machine has been used. The machine worked in displacement control. The shape of ramp displacement is linear and 0.1 mm/min is the definition.

Appendix C figure 2 Instron 8501

The procedure that has been used consists in a tensile test to define the characteristic curve of material. The specimens are too little and the use of an extensometer is not possible. In this test campaign a camera has been used. The machine and the camera are connected to the computer. The program Easy DAQ v.3.2B read and save the force that the machine uses and converts it from Volt to mm or MPa. The program Eye Cockpit UI149xSE-C captures and analyses the pictures that have been taken from the camera. The pictures have been analysed to define the little diameter in every picture. This information has been used to define the real tension and deformation. The diameters of specimens are:

	E1	E2	E3	E4
Diameter [mm]	2.98	3.03	2.94666	3
F max [KN]	15.78	15.85	15.69	16.04

Appendix C tabella results 1

For every test we have the time, the load on KN, the minimum diameter in pixel and the position of the minimum diameter. The measure of diameter must be converted in mm and the true stress and strain could be defined with the following formulas.

$$\varepsilon_{true} = \ln\left(\frac{\varepsilon_0}{\varepsilon}\right)$$

$$\sigma_{true} = \frac{F}{A_{true}}$$

For every specimen these results have been plotted. The behaviour of every specimen is similar and the material chart chosen is:

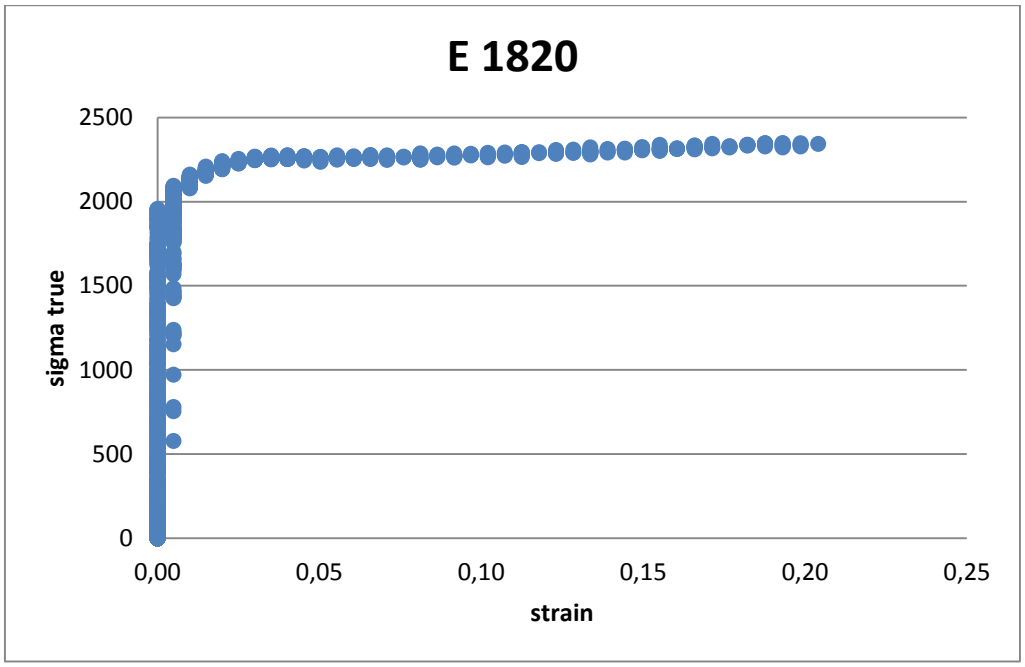

Appendix C figure 3 Material

Index:

References

- The Theory of Critical Distances: A New Perspective in Fracture Mechanics - David Taylor. Elsevier Science Ltd; 1 edition (30 May 2007).
- Ashby, M.F. and Jones, D.R.H. (2005) Engineering materials I. Elsevier, Oxford UK.
- Atzori, B., Lazzarin, P., and Filippi, S. (2001) Cracks and notches: Analogies and differences of the relevant stress distributions and practical consequences in fatigue limit predictions. International Journal of Fatigue 23, 355-362
- Broberg, K.B. (1999) Cracks and fracture. Academic Press, London UK.
- Bruckner-Foit, A., Huang, X., and Motoyashiki, Y. (2004) Mesoscopic simulations of damage accumulation under fatigue loading. In Proceedings of the 15th European Conference of Fracture (Edited by Nilsson, F.) pp. 3-12. KTH, Stockholm, Sweden.
- Creager, M. and Paris, P.C. (1967) Elastic field equations for blunt cracks with reference to stress corrosion cracking. International Journal of Fracture Mechanics 3,247-252.
- Delaire, F., Raphanel, J.L., and Rey, C. (2000) Plastic heterogeneities of a copper multicrystal deformed in uniaxial tension: Experimental study and finite element simulations. Acta Mater. 48, 1075-1087.
- Filippi, S. and Lazzarin, P. (2004) Distributions of the elastic principal stress due to notches in finite size plates and rounded bars uniaxially loaded. International Journal of Fatigue 26, 377-391.
- Hertzberg, R.W. (1995) Deformation and fracture mechanics of engineering materials. Wiley, New York USA.

- Irwin, G.R. (1964) Structural aspects of brittle fracture. Applied Materials Research 3,65- 81. Janssen, M., Zuidema, J., and Wanhill, R. (2002) Fracture mechanics. Spon, London UK. Knott, J.F. (1973) Fundamentals of fracture mechanics. Butterworths, London.
- Murakami, Y. (1987) Stress intensity factors handbook. Pergamon, Oxford UK.
- Neuber, H. (1958) Theory of notch stresses: Principles for exact calculation of strength with reference to structural form and material. Springer Verlag, Berlin.
- Paris, P.C. (1964) Fatigue - An interdisciplinary approach. In Proc. 10th Sagamore Conference pp. 107-117. Syracuse University Press, Syracuse, New York USA.
- Peterson, R.E. (1974) Stress concentration factors. Wiley, New York USA.
- Westergaard, H.M. (1939) Bearing pressures and cracks. Journal of Applied Mechanics A 49-53. Williams, M.L. (1952) Stress singularities resulting from various boundary conditions in angular corners of plates in extension. Journal of Applied Mechanics 19, 526-528.
- Wulpi, D.J. (1985) Understanding how components fail. ASM, Ohio USA.
- http://www.dynasupport.com/howtos/element/cohesive-element-formulation
- Japan Concrete Institute Standard: Method of test for fracture energy of concrete by use of notched beam JCI-S-001-2003.
- M.R. Ayatollahi , A.R. Torabi (2010): Tensile fracture in notched polycrystalline graphite specimens Fatigue and Fracture Research Laboratory, Center of Excellence in Experimental Solid Mechanics and Dynamics, Department of Mechanical Engineering, Iran University of Science and Technology, Narmak, 16846 Tehran, Iran.

- C. Landron , E. Maire , J. Adrien , O. Bouaziz : Damage characterization in Dual-Phase steels using X-ray tomography. T. Proulx (ed.), Optical Measurements, Modelling, and Metrology, Volume 5, Conference Proceedings of the Society for Experimental Mechanics Series 9999999, DOI 10.1007/978-1-4614-0228-2_2, © The Society for Experimental Mechanics, Inc. 2011.
- Alfred Cornec, Ingo Scheider, Karl-Heinz Schwalbe: On the practical application of the cohesive model. Institute for Materials Research, GKSS Research Centre Geesthacht, Max-Planck-Strasse 1, 21502 Geesthacht, Germany Received 11 November 2002; received in revised form 12 March 2003; accepted 12 March 2003.
- J. Planas , M. Elices, G.V. Guinea, F.J. Gomez, D.A. Cend on, I. Arbilla: Generalizations and specialization s of cohesive crack models. Engineering Fracture Mechanics 70 (2003) 1759–1776.
- J.M. Sancho, J. Planas, D.A. Cendo´n, E. Reyes, J.C. Ga´lvez: An embedded crack model for finite element analysis of concrete fracture. Engineering Fracture Mechanics 74 (2007) 75–86
- D.A. Cendón, F. Berto2 P. Lazzarin and M. Elices: EXTENSION OF THE COHESIVE CRACK MODEL TO PMMA NOTCHED SPECIMENS EXHIBITING A NON LINEAR BEHAVIOUR UNDER TORSION.
- K. Taghizadeh, F. Berto , E. Barati: Local strain energy density applied to martensitic steel plates weakened by U-notches under mixed mode loading. Theoretical and Applied Fracture Mechanics 59 (2012) 21–28.
- F.J. Gómez, M. Elices, F. Berto, P. Lazzarin: A generalised notch stress intensity factor for U-notched components loaded under mixed mode. Engineering Fracture Mechanics 75 (2008) 4819–4833.

- F.J. Gomez, M. Elices, J. Planas: he cohesive crack concept: application to PMMA at -60°C. Engineering Fracture Mechanics 72 (2005) 1268–1285.
- F.J. Gomez, M. Elices: Fracture of components with V-shaped notches. Engineering Fracture Mechanics 70 (2003) 1913–1927.
- F.J. Gómez, M. Elices, F. Berto, P. Lazzarin: Fracture of U-notched specimens under mixed mode: Experimental results and numerical predictions. Engineering Fracture Mechanics 76 (2009) 236–249.
- F. Berto, P. Lazzarin: Recent developments in brittle and quasi-brittle failure assessment of engineering materials by means of local approaches. Materials Science and Engineering R 75 (2014) 1–48.
- LS-DYNA® KEYWORD USER'S MANUAL VOLUME I-II (2012) LIVERMORE SOFTWARE TECHNOLOGY CORPORATION (LSTC).
- F.J. Gómez, M. Elices and A. Valiente: Fracture of a high strength steel containing U-notches.
- GIULIO FIORETTO: tesi di laurea magistrale low temperature tests on pmma notched bars subjected to torsion. Università degli studi di Padova (2013)
- Marcon Marco: static tests under torsion loading of notched specimens made of grey cast iron: experimental issues and numerical development. università degli studi di padova (2014).
- A.R. Torabi e M. Alaei: Application of the Equivalent Material Concept to ductile failure prediction of blunt V-notches encountering moderate-scale yielding

Ringraziamenti:

- Vorrei ringraziare il prof. Filippo Berto per aver reso possibile il lavoro descritto in queste pagine, per la sua disponibilità e per quello che mi ha trasmesso nel periodo in cui ho studiato qui a Vicenza
- Voglio ringraziare con tutto il cuore il prof. David Cendón per la disponibilità, la pazienza e la simpatia dimostratami e per tutto quello che mi ha insegnato durante il mio lavoro a Madrid. Un grazie anche ai raggazzi dell'officina meccanica per l'aiuto che mi hanno sempre dato e ai ricercatori e professori del Dipartimento di Scienza dei materiali della UPM.
- Vorrei anche ringraziare il prof. Paolo Lazzarin che nei suoi corsi ci ha trasmesso il rispetto e l'amore per la meccanica dei materiali.
- Vorrei ringraziare i miei genitori e le mie sorelle per il supporto datomi e per avermi sopportato durante questi anni.
- Un grazie alla nonna Rosy per tutte le raccomandazioni a Dio che ha fatto.
- Un grazie a Laura per la pazienza che mi ha dimostrato durante la stesura della tesi.
- Un grazie al dott. Sebastino Rizzardo che con il suo esempio mi ha dimostrato che con l'impegno e la tenacia ogni obbiettivo è raggiungibile.
- Un grazie a tutti gli amici che in questi anni mi hanno accompagnato permettendomi di non smarrire la via della Volgia, grazie non vi cito tutti perchè sarebbe dispersivo.
- Ringrazio Marjolyn Consolaro per il supporto tecnico nella correzione della sintassi.